Final Report on

Improving Understanding and Prediction of Warm Season Precipitation Systems in the Southeastern and Mid-Atlantic Regions

to the
National Oceanic and Atmospheric Administration
Collaborative Science, Technology & Applied Research Program (CSTAR)
Award Number NA07NWS4680002

Department of Marine, Earth, & Atmospheric Sciences
North Carolina State University
Raleigh, North Carolina

July 2011

Contact Person: Gary M. Lackmann
Department of Marine, Earth, & Atmospheric Sciences
Box 8208
North Carolina State University
Raleigh, North Carolina 27695-8208
Phone: (919) 515-1439
Fax: (919) 515-7802
gary@ncsu.edu

List of Participants and Collaborators:

Principal Investigators - North Carolina State University:
Dr. Gary Lackmann
Dr. Matthew Parker
Dr. Lian Xie

Student Researchers:
Mr. Adam Baker – Graduated (MS) 2009
Ms. Casey Letkewicz – Graduated (MS) 2009
Mr. Matt Morin – Graduated (MS) May 2011
Ms. Qianhong Tang – Graduated (PhD) 2010

Collaborative Offices of the National Weather Service:
Raleigh, North Carolina
Wilmington, North Carolina
Morehead City, North Carolina
Blacksburg, Virginia
Sterling, Virginia
Wakefield, Virginia
Greer, South Carolina
Charleston, South Carolina
Columbia, South Carolina
Peachtree City, Georgia

A. Overview and Summary of Work

The original proposal outlined four main areas of research: (i) warm-season cold-air damming (CAD) and wedge-front convection, (ii) mesoscale convective systems (MCSs) crossing the Appalachian Mountains, (iii) tornadoes accompanying landfalling tropical cyclones, and (iv) tropical cyclone quantitative precipitation forecasting (QPF), and hydrological modeling. The proposed work was completed during a 4-year period that included a 1-year no-cost extension, which was motivated by the participation of PI Parker and graduate student Matt Morin in the Vortex2 field program during spring of 2009 and spring 2010. Each of the four research projects was completed, and four graduate students earned their degrees with support from this award.

In the sections that follow, a summary of main operational and scientific findings will be presented. A brief set of highlights are provided below.

- Three recorded presentations were made (Baker, Letkewicz, and Morin) highlighting the operationally relevant findings from the project. These presentations and other CSTAR research updates can be found at http://www.meas.ncsu.edu/nws/www/resupdates/. See also the new site: http://sites.google.com/site/nwsncsucollab/home/publications/cstar-projects.
- Four site visits were conducted by students working on the project, including trips to Blacksburg VA and Peachtree City, GA.

- A total of 8 seminars presenting work from the project were delivered by students working on the project.
- Five conference presentations were delivered highlighting project-related research findings.
- Casey Letkewicz presented "An Investigation of Mesoscale Convective Systems Crossing the Appalachian Mountains" with Dr. Matt Parker at AMS Severe Local Storms Conference. Casey won the award for best student poster.
- Dr. Matt Parker taught a 3-hour short course in March, 2009 as part of the NWS RAH severe weather training week series.
- Four graduate students completed their degrees with support from this award, including 3 M.S. students and 1 Ph.D. student.
- An overview of research was presented at a CSTAR workshop in October 2010, hosted by the NWS-Raleigh and NCSU. A complete set of presentations is available at http://cimmse.wordpress.com/2010/11/01/2010-cstar-workshop/.

B. Research Results

i.) Wedge-front convection (Baker and Lackmann)

The main objectives of this research component are as follows:

Objective 1: **Improve understanding of the character of the lower troposphere in the vicinity of the wedge front during events with peripheral convection.** The original hypothesis was that a linkage exists between the strength of the thermal gradient at the wedge front and the vertical shear at the periphery of the cold dome, via the thermal wind relation. Thus, provided that instability can be accurately forecast, the prediction of severe wedge front convection is tied to reliable prediction of the CAD event itself. In the warm season, abundant moisture and instability are typically found surrounding the CAD air mass, and the convergent flow near the wedge front provides a lifting mechanism. We must also differentiate wedge-front conditions that are characterized by active, severe convection from those events which are inactive.

Objective 2: **Improve understanding and numerical prediction of CAD erosion.** Intense summertime solar radiation and observations of previous warm-season CAD events demonstrates the complexity of this forecast problem. Model physics interactions, including those related to the PBL, radiation, cloud and precipitation physics, and convective parameterization, are crucial to the ability of models to represent the CAD erosion process.

The thesis project of Adam Baker emphasized Objective 1, which was the primary objective of this research component. Additional research by PI Lackmann addressed Objective 2, although this aspect is not emphasized in this report.

Objective 1: The influence of CAD on convection and the convective environment

The relation of CAD to convection and the convective environment was viewed as the primary research objective of this project component. Adam Baker defended his M.S. thesis on this topic on 17 July 2009, and has since given three oral presentations and one recorded presentation of the results. Our goals in this subsection were (i) to distinguish the synoptic- and mesoscale environments for CAD events with and without severe peripheral convection, and (ii) for convectively active events, better understand the effect of the wedge front on the convective environment.

The first step was to conduct a climatological study in order to gauge the frequency and importance of convection in the vicinity of a CAD event. The results demonstrate that approximately 10% of CAD days were accompanied with wedge-front convection, which was defined as radar reflectivity of at least 35 dBz within 100 km of a subjectively analyzed wedge front. Of the active wedge-front convection days, 50% occurred during the spring months of March, April, and May, 36% occurred from July to October, and 14% occurred in January and February (not shown). This provides valuable context for case studies, and allows the construction of composites for convectively active and inactive CAD events.

After building a sufficient sample of active wedge-front convection events, the cases were stratified into those involving a relatively strong, well-defined CAD cold dome and those with weaker CAD signals. Of all the wedge-front convection events, 8 cases stood out as being characterized by a strong CAD cold dome; a representative event was the 20 March 2003 case. Such a case presented an opportunity to isolate the effects of a CAD cold dome on the lower-tropospheric environment for convective development. We hypothesize that the presence of a CAD cold dome alters the environment in a way that makes an appreciable difference in convective character and intensity. This has been known to forecasters, or assumed to be correct, but we sought to isolate and quantify the CAD contribution to environmental changes at the wedge front.

In order to isolate the role of the wedge front in this event, numerical simulations of the 20 March 2003 case were undertaken. A control simulation was able to accurately reproduce the CAD event and trigger convection near the wedge front (Fig. 1.1a). An experimental simulation in which the mountains were removed was compared to the control in order to quantify differences in instability, shear, and lift in the vicinity of the observed wedge front. In this run, the region of convective triggering was displaced towards the coast relative to the control run (Fig. 1.1b).

With these model runs available, we were able to quantify differences in the convective environment between the runs, and isolate the role of the front in convective activity. Prior to analysis of these model runs, we hypothesized that (a) the presence of CAD would serve to stabilize the environment, mostly in the interior of the CAD cold dome, (b) the increase in vertical shear near the periphery of the cold dome would lead to an environment more favorable for rotating storms there, and (c) that surface convergence and lift in the vicinity of the wedge front could serve as a trigger for convective initiation there.

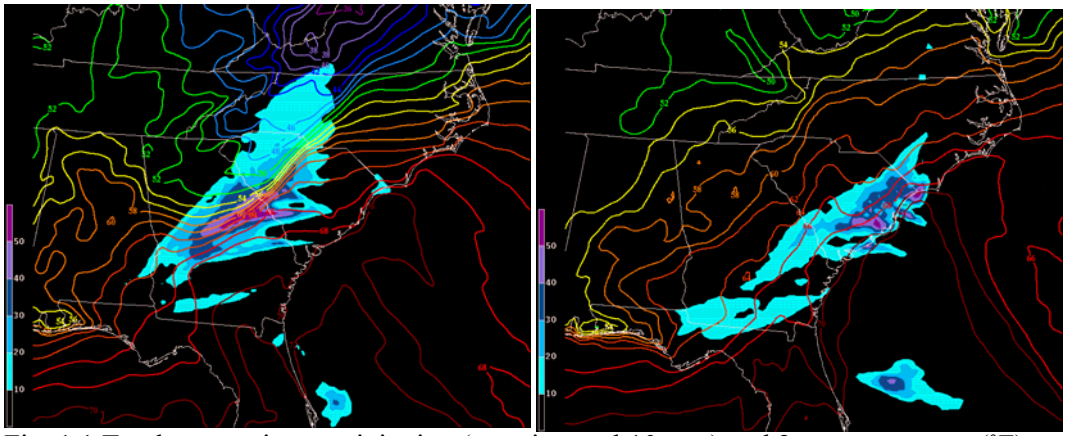
Fig. 1.1 Total convective precipitation (mm, interval 10 mm) and 2-m temperature (˚F) at 12 UTC 20 March 2003 (hour 54) for (a) control and (b) experimental run.

Figure 1.2 confirms that as expected, the model simulation with CAD was characterized by a more stable environment, especially within the core of the cold dome. While the presence of CAD may limit instability, a large positive difference in lower-tropospheric (0-1 km) wind shear (helicity) is also observed, again consistent with hypotheses (Fig. 1.2). While some of the shear increase coincides with very stable air, the helicity difference field over northern and central Georgia overlaps with unstable air in areas where convection was observed, and where it was triggered in the control simulation (Figs. 1.1, 1.2). The difference field of helicity shown in Fig. 1.2c is consistent with expectations.

A third hypothesis relates to the role of the CAD wedge front as a convective trigger. Either near-surface convergence in the immediate vicinity of the wedge front, or isentropic lift as moist southerly or southeasterly flow overrides the cold dome could serve to initiate convection. Comparison of vertical motion and convergence between the control and experimental simulations reveals that the wedge front indeed provides a significant lifting mechanism (Fig. 1.3). In addition, both runs show convergence and ascent along the coastline (most likely frictional convergence); however the area of strongest ascent and convergence is located near the wedge front in the control simulation.

While the relatively coarse 12-km WRF simulations presented above are useful in isolating differences in the convective environment attributable to the presence of CAD, there are unanswered questions regarding the specific behavior of convection with and without the presence of CAD. Two important questions that can be addressed with higher resolution model runs are:

- To what extent does the helicity-rich air from within the wedge-frontal zone become incorporated into convective updrafts? What environmental or storm-scale processes regulate the ability of storms to draw on the potential rotation?
- What is the maximum grid length at which an operational forecast model could be run to explicitly capture wedge-front convection? Or, is a relatively coarse simulation with parameterized convection adequate to predict such events?

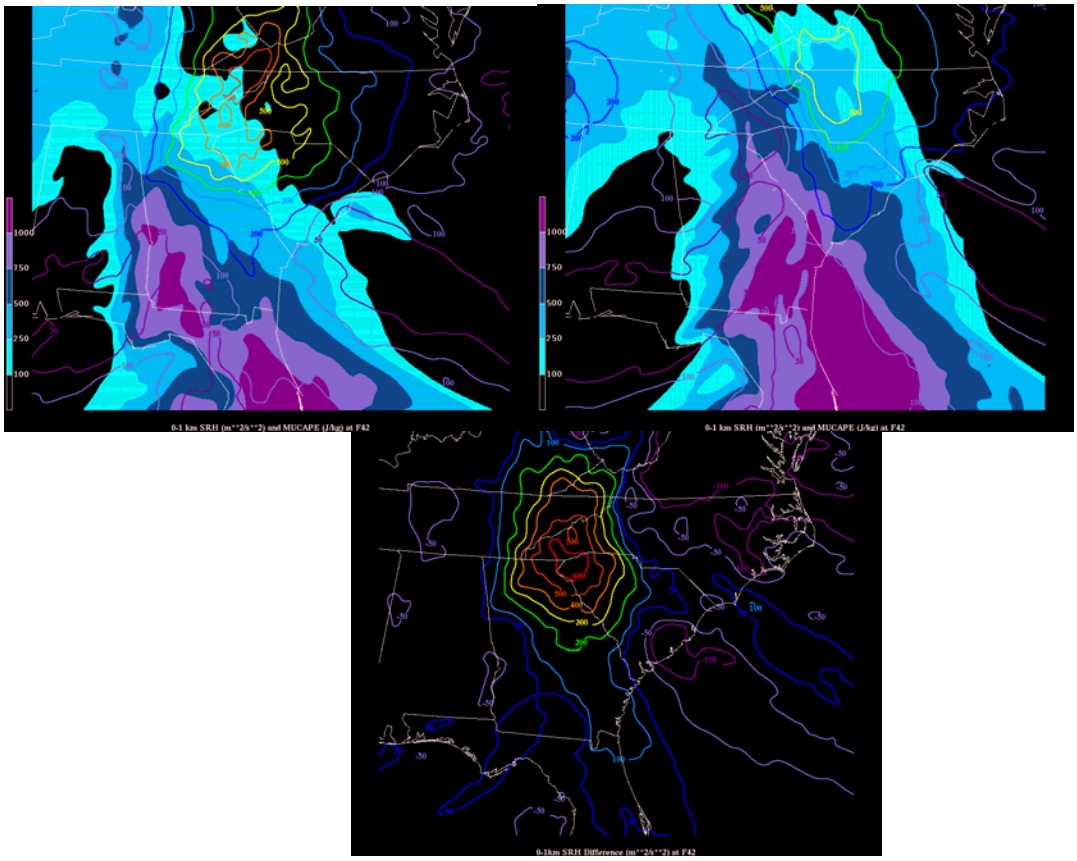

Fig. 1.2. Most-unstable convective available potential energy (MUCAPE, J/kg, shaded) and 0-1 km storm-relative helicity (m^2/s^2, contoured) at 00 UTC 20 March 2003 (hour 42) for (a) control and (b) experimental run. The light blue shading is at least 100 J/kg, dark blue is at least 500 J/kg, and the darker purple is at least 1000 J/kg. (c) is the difference in 0-1 km SRH between the runs.

In order to address these questions, additional model runs were performed with nesting down to 1.3 km horizontal grid spacing (Fig. 1.4a).

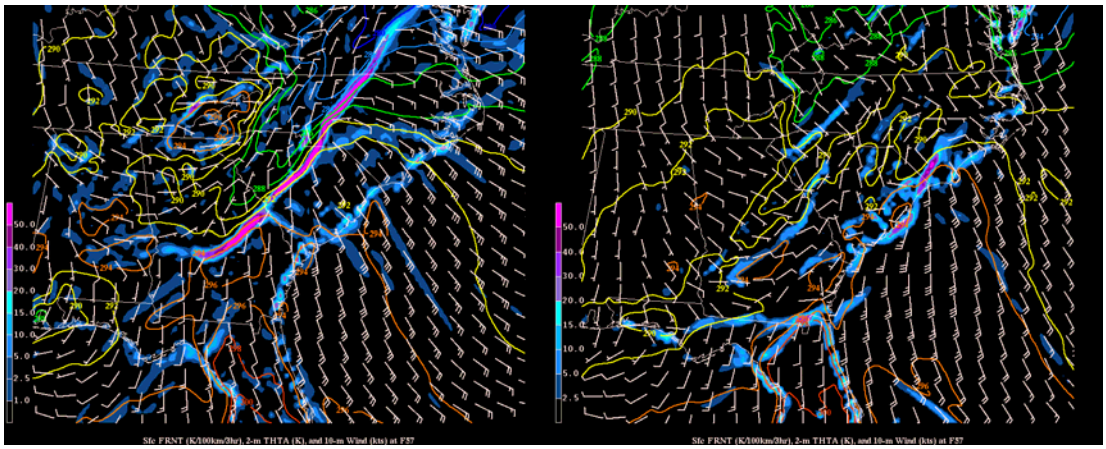

Fig. 1.3. Potential temperature at 2 meters (contours), frontogenesis function (color filled), and 10-m wind barbs (kt) at 15 UTC 20 March 2003 (hour 57 of the simulation) for (a) control and (b) experimental (no-CAD) run.

The results of the high-resolution simulations reveal the development of splitting, rotating storms forming along the CAD wedge-front boundary (Figs. 1.4b-d). The right-moving cell shown in Fig. 1.4d was found to produce a strong rotating updraft (not shown), consistent with expectations for convection forming in a sheared environment of this type.

However, unexpected findings resulted from a similar high-resolution model simulation from the no-CAD setup. Here, rotating storms also formed, presumably due to the larger CAPE in conjunction with the presence of a veering wind profile associated with warm advection that was taking place independent of the CAD event (not shown). This finding suggests that at least in this particular event, the presence of the CAD cold dome and wedge front were perhaps *not* critical to the occurrence of rotating convection. We speculate that it may be cases in which marginal shear is available that the wedge front plays the most critical role in the formation of rotating storms.

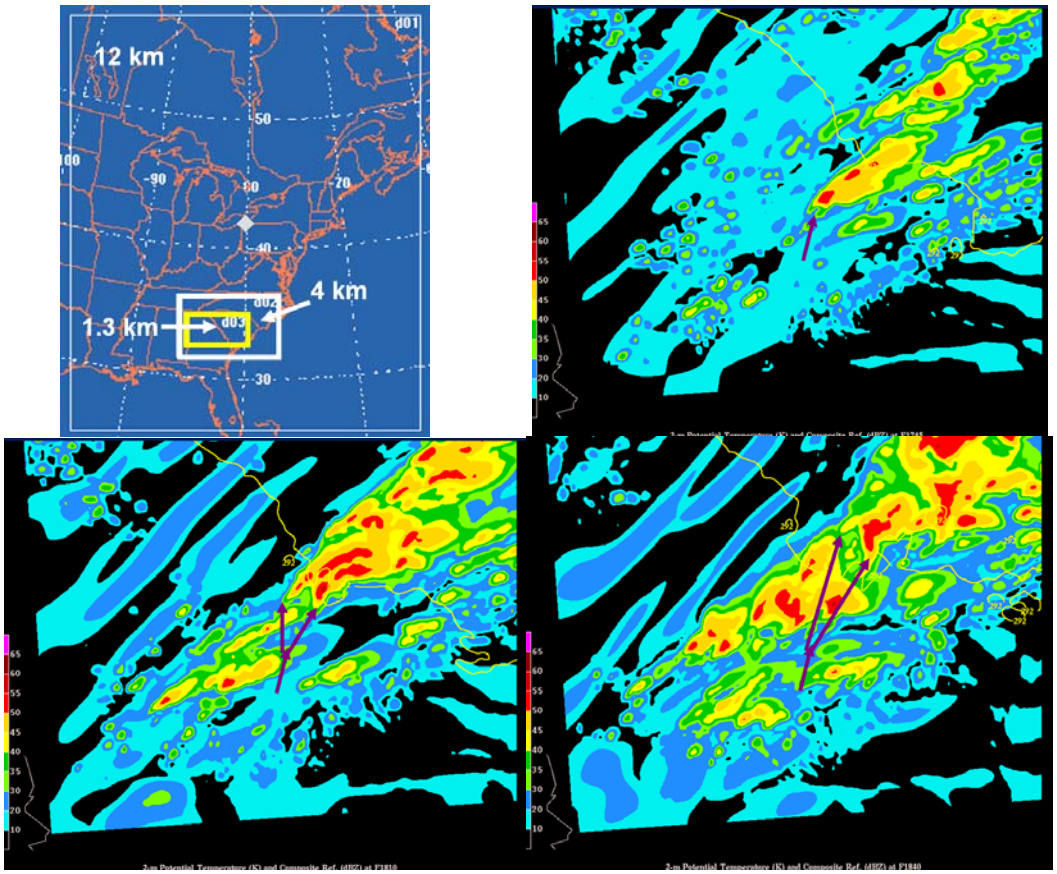

Fig. 1.4. (a) WRF domain configuration for high-resolution convection-resolving simulations of wedge-front convection for 20 March 2003 case study; (b), (c), and (d) depict model simulated composite radar reflectivity from 1.3 km domain for control (with CAD) WRF simulation. The three snapshots (and purple arrows) show the evolution of a splitting, rotating storm that formed in the vicinity of the wedge front.

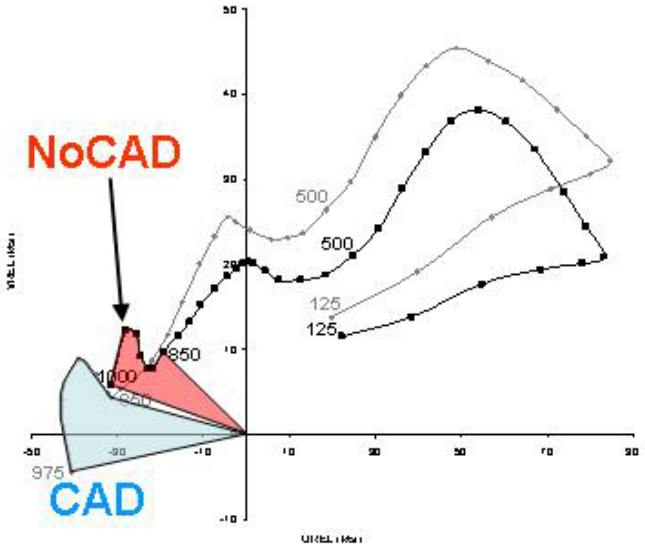

Figure 1.5. Averaged storm-relative hodographs (kt) from points along region of convective development at times 5 min before initial convective development was analyzed in the CAD-CS (blue) and NoCAD-CS (red) runs for times valid at 20 March 2003 0500Z and 0615Z, respectively (forecast times of 47 hrs 0 min and 48 hrs 15 min). Select hodograph points labeled in mb. Lower left points of hodographs represent the highest pressure level outputted from the model sounding calculations and shaded regions outline the approximate amount of storm-relative helicity from these points up to the 850-mb-level.

Comparison of simulated reflectivity between the runs indicated more discrete cell development in the CAD run, while convection had a more linear development in the NoCAD run. The low-level shear environment along the development regions of the storms was more favorable for rotating updrafts along the wedge front, as evident from enhanced 0-1-km storm-relative helicity (SRH) values in CAD run (Fig. 1.5). While significant updraft rotation was present in both runs, quantification of convective intensity over time revealed that the convection was cell-for-cell more intense *without* the presence of the wedge front (Fig. 1.6). This was attributed to increased updraft speeds associated with the more unstable environment in the NoCAD run. Increased low-level SRH associated with the cold dome in this case *failed* to compensate for the loss of instability with the ingredients needed for the development of strong rotating convection along the wedge front. While this result may at first appear surprising, it is important, because it reveals that the presence of the CAD, can serve to diminish the severity of convection in situations where the environment is marginally conducive to convection. This is not the case for all CAD events, however.

Although the cold dome provided strong low-level shear, this was a case characterized with both high instability and strong deep-layer shear would have likely developed strong rotating convection even *without* the presence of the wedge front. The role of the front in this case served primarily to influence the *location*, rather than severity, of the convection. We speculate that cases characterized by relatively weak deep-layer shear, but with strong instability, would be more likely to show a prominent role for the wedge front. With weak 0-6-km shear, convection may not develop strong rotation unless cells were able to tap the helicity-rich low-level shear environment associated with the presence of the wedge front.

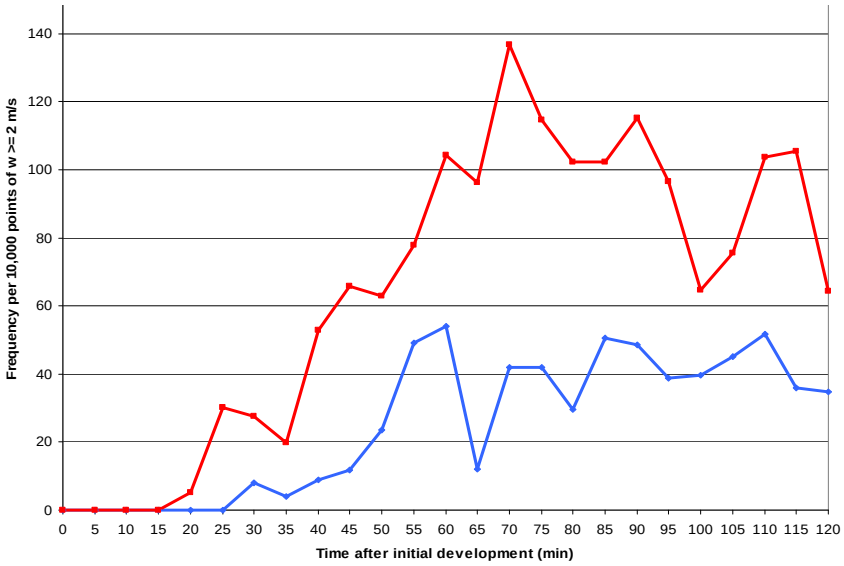

Figure 1.6. Frequencies of updraft rotation ≥ 1000 x 10^{-4} m/s^2 normalized across grid cells of vertical velocity ≥ 2 m/s for 2 hrs following initial convective development: CAD-CS (blue) and NoCAD-CS (red). Values per 10,000 grid cells with w ≥ 2 m/s. CAD-CS run data are valid from 20 March 2003 0505Z to 0705Z (forecast times of 47 hrs 5 min to 49 hrs 5 min). NoCAD-CS data are valid from 20 March 2003 0620Z to 0820Z (forecast times of 48 hrs 20 min to 50 hrs 20 min).

With this finding, we again drew upon the earlier climatological case archive to better establish the spectrum of wedge-front convection events. The 24 previously identified wedge-front convection events were stratified by upstream instability (SBCAPE) and deep-layer (0-6-km) shear values (Fig. 1.7). In this diagram, the environment in the upper-right portion of the diagram is conducive to severe convection, even without the presence of the wedge front (large shear and strong instability are present in the environment). However, cases found in the upper-left portion of the spectrum are those in which the presence of the wedge front is expected to play a more critical role; these events are characterized by strong instability but otherwise weak environmental shear. The occurrence of severe weather on four of these days may be related to the addition of shear in the vicinity of the wedge front.

In light of the climatological spectrum, we recognized the need to repeat our earlier model experiments with an event from the upper-left portion of the spectrum. Additional results from experiments using the 11 May 2002 CAD event – a case with high instability and contrastingly weak deep-layer shear, have now been obtained. Initial 12-km simulations indicate a similar lower-tropospheric influence of the cold dome on the convective environment as in the first case. While discrete pulse-like storms developed in the presence of the wedge front, no significant convection was triggered in the comparable region after CAD was removed. The cold dome was analyzed to noticeably enhance the helicity of the low-level environment in the storm development region, supporting the proposed conceptual model.

In summary, by using numerical experiments to examine specific CAD convective events, we have been able to quantify the precise role of CAD in the convective

environment. The role of CAD is found to vary considerably in different cases, making the strongest contribution to severe convection in shear-limited events with sufficient instability.

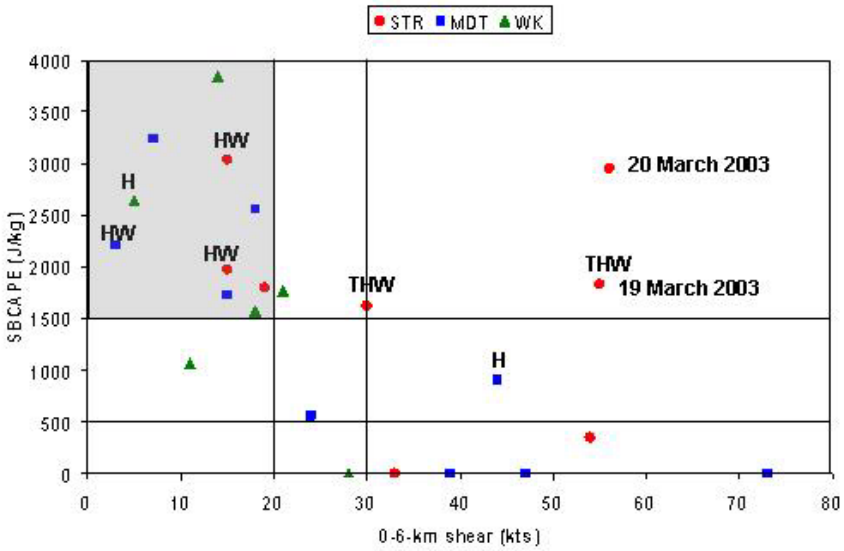

Figure 1.7. Stratification of WFC days from case dataset by SBCAPE (J/kg) and 0-6-km shear (kt) from modified sounding data at Tallahassee, FL (TLH), typically upstream of WFC. Relative strength of cold dome associated with the WFC is included as weak (WK, green triangles), moderate (MDT, blue squares), or strong (STR, red circles). Days associated with severe convection are labeled for types of severe reports with "H" for hail, "W" for damaging wind, and "T" for tornado. Dates of WFC included in the simulated CAD event are labeled (19 and 20 March 2003). Most common scenario is shaded: SBCAPE > 1500 J/kg and 0-6-km shear < 20 kt.

On 3 June 2009, Adam presented the latest research at the 23rd Conference on Weather Analysis and Forecasting/19th Conference on Numerical Weather Prediction in Omaha, NE. The presentation recording and PDF of the extended abstract are available online at http://ams.confex.com/ams/23WAF19NWP/techprogram/session_23128.htm. He successfully defended his Master's thesis and passed the oral exam unconditionally on 17 July 2009, and the thesis was accepted into the NCSU graduate school on 31 Aug. 2009 (electronic PDF available online at http://www.lib.ncsu.edu/theses/available/etd-08172009-161547/).

Since then, Adam has prepared a research update in the form of a narrated Articulate PowerPoint presentation (recorded on 24 Sept. 2009 and available online) with the help of Jonathan Blaes (SOO, NWS WFO Raleigh, NC) to share the final thesis results and gather feedback from the NWS. On 2 Oct. 2009 Adam traveled to Peachtree City, GA to present the research results to the NWS WFO and Southeast River Forecast Center staff and gain useful feedback (invited by Steve Nelson, SOO and forecaster Trisha Palmer of the WFO). Adam began work as a NWS employee at the Indianapolis, IN forecast office in December, 2009. He presented this research at the National Weather Association 14th Annual Severe Storms and Doppler Radar Conference, Des Moines, IA, 27 March 2010. Adam also presented a summary of his work remotely at the October 2010 CSTAR meeting in Raleigh.

Objective 2: Model processes and CAD erosion

PI Lackmann presented work on CAD erosion at the 22nd AMS conference on Weather Analysis and Forecasting held in Omaha, NE in 2009. A CAD event in which numerical forecasts were not successful took place on 29-30 October, 2002. Earlier research as part of a previous CSTAR project by the PI and Wendy Sellers (now Wendy Moen of the Charleston, SC NWS Forecast Office) had identified issues with cloud-radiation interactions as well as with overactive mixing by the shallow convective component of the BMJ convective parameterization scheme as responsible for premature erosion of the CAD cold dome. These earlier research simulations were conducted with the MM5 and Eta models, and it was not clear that the results carried over to the newer models such as the Weather Research and Forecasting (WRF) model. A series of experiments were conducted using the WRF model with different PBL and convective scheme options, and it was found that none of the model simulations produced the severity of the error in the operational Eta forecasts from October 2002 (Fig.1.8a). The improvement is likely related to elimination of an error in cloud-radiation interactions as well as to modification of the shallow mixing component of the BMJ scheme, although it is not possible to rule out other model improvements as contributing as well.

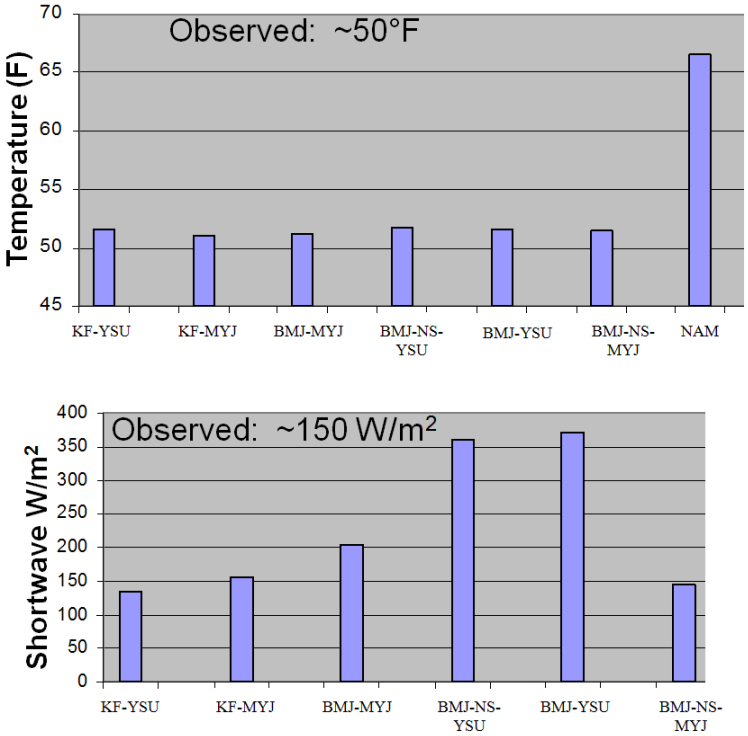

Fig. 1.8. Comparison of WRF area-averaged surface temperature forecasts with operational NAM forecasts (top panel); comparison of surface shortwave radiation for the same set of model runs, but without the NAM (for which this parameter was not available).

The importance of model physics interactions was evident in these simulations. The Yonsei University PBL scheme (YSU) includes a moist entrainment formulation that can account for mixing due to shallow, non-precipitating convection near the PBL top. The

BMJ CP scheme also has a shallow mixing formulation that accounts for similar processes. Model runs with the shallow BMJ disabled, or runs with the Mellor-Yamada-Janjic (MYJ) PBL scheme didn't produce as much mixing near or above the PBL (Fig. 1.9). Furthermore, runs with the full BMJ and YSU scheme demonstrated redundancy in representation of the shallow mixing process (Fig. 1.9a). These experiments suggest that an optimal model configuration for CAD prediction would be a BMJ-MYJ CP/PBL combination. This is the same physics suite that is run in the operational NAM, although caution must be used in comparing results in different modeling systems.

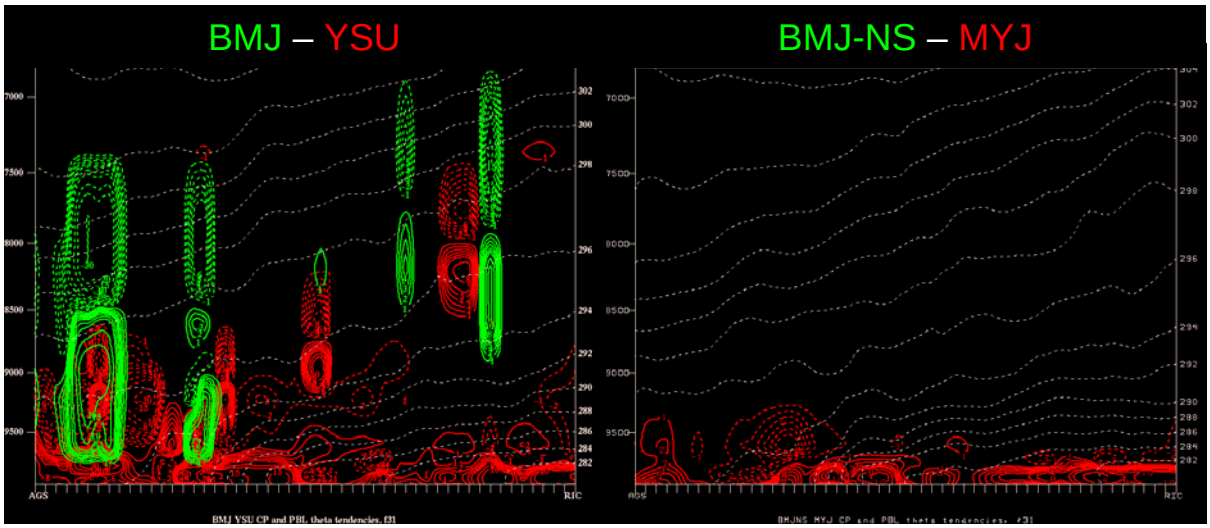

Fig. 1.9. (a) Potential temperature tendency in the lower troposphere from the BMJ CP scheme (green) and YSU PBL scheme (red); dashed values are negative. (b) As in (a) except for run with BMJ shallow mixing disabled.

ii.) MCS interactions with the Appalachian Mountains (Letkewicz and Parker)

When a strong MCS is present to the west of the Appalachian Mountains, forecasters in regions east of the mountains are confronted by the question of whether or not the system will maintain strength when crossing the mountains. Preliminary work that motivated this component of our CSTAR proposal was presented by Parker and Ahijevych (2007), who documented the frequencies and typical properties of MCSs in the eastern U.S., including those approaching the Appalachian Mountains from the west. Of particular relevance to this present study, Parker and Ahijevych showed that roughly 14 MCSs per year cross the Appalachians from west to east; Keighton et al. (2007) noted that these are often implicated in widespread severe weather in the lee of the mountains.

Graduate student Casey Letkewicz worked with PI Parker on this aspect of the project. An initial step was to understand the environmental differences that discriminate between MCSs that do vs. do not cross the Appalachians. The culmination of Casey's work involved numerical model simulations of idealized MCSs crossing mountain barriers; simulations were designed to improve understanding of the fundamental processes at work during these events.

During the course of her M.S. work, Casey actively interacted with NOAA/NWS personnel, including several conference calls with Steve Keighton (NWS-Blacksburg) as well as site-visit to NWS-Blacksburg and a presentation at the NWS-Raleigh office. She defended her M.S. thesis in April 2009. Since the completion of her M.S. degree, Casey has been working towards her doctoral degree under the continued advisement of Dr. Parker.

CSTAR scientific outcomes:

The first part of this study examined twenty crossing and twenty noncrossing MCSs encountering the Appalachian Mountains. Statistical analysis of representative inflow soundings upstream and downstream of the mountains revealed that the ***downstream environment*** discriminated better between crossing and noncrossing cases than did upstream conditions. Crossing cases in particular were associated with much higher CAPE and less CIN in the lee, in addition to less vertical wind shear and a weaker mean wind. The role of CAPE in maintaining convection is well-understood and is unsurprisingly associated with mature MCSs (e.g. Coniglio et al. 2007; Cohen et al. 2007). The role of the wind profile was not as clear, particularly since mature MCSs are often associated with higher vertical shear and mean wind values. Two hypotheses were proposed to explain the role of the wind profile: 1) because an MCS's cold pool is weakened as it traverses the barrier, a weaker vertical wind shear is more nearly in balance with the outflow in the lee, thus promoting deeper lifting according to the theory of Rotunno et al. (1988); and 2) a weaker mean wind results in weaker downslope flow in the lee, leading to less suppression of the convection as it descends the mountain. These two hypotheses were then tested using idealized numerical simulations with experiments centered on the wind profile. One set of experiments increased and decreased the mean wind of an idealized wind profile while another set increased and decreased the low-level

shear. A final set of experiments incorporated the composite observed crossing and noncrossing wind profiles.

Results of the modeling tests revealed that despite any changes to the idealized or observed wind profile, a crossing MCS was always simulated. Changes to the mean wind produced more or less orographic enhancement and convective suppression in the lee (cf. Figs. 2.1a-c) and while changes to the low-level shear primarily impacted updraft tilt and the system's organization (Figs. 2.2 and 2.3), though due to the inherent correlation between shear and the mean wind, changes to the low-level shear also produced fluctuations in convective intensity as the system traversed the barrier as a result of larger or smaller mean wind speeds.

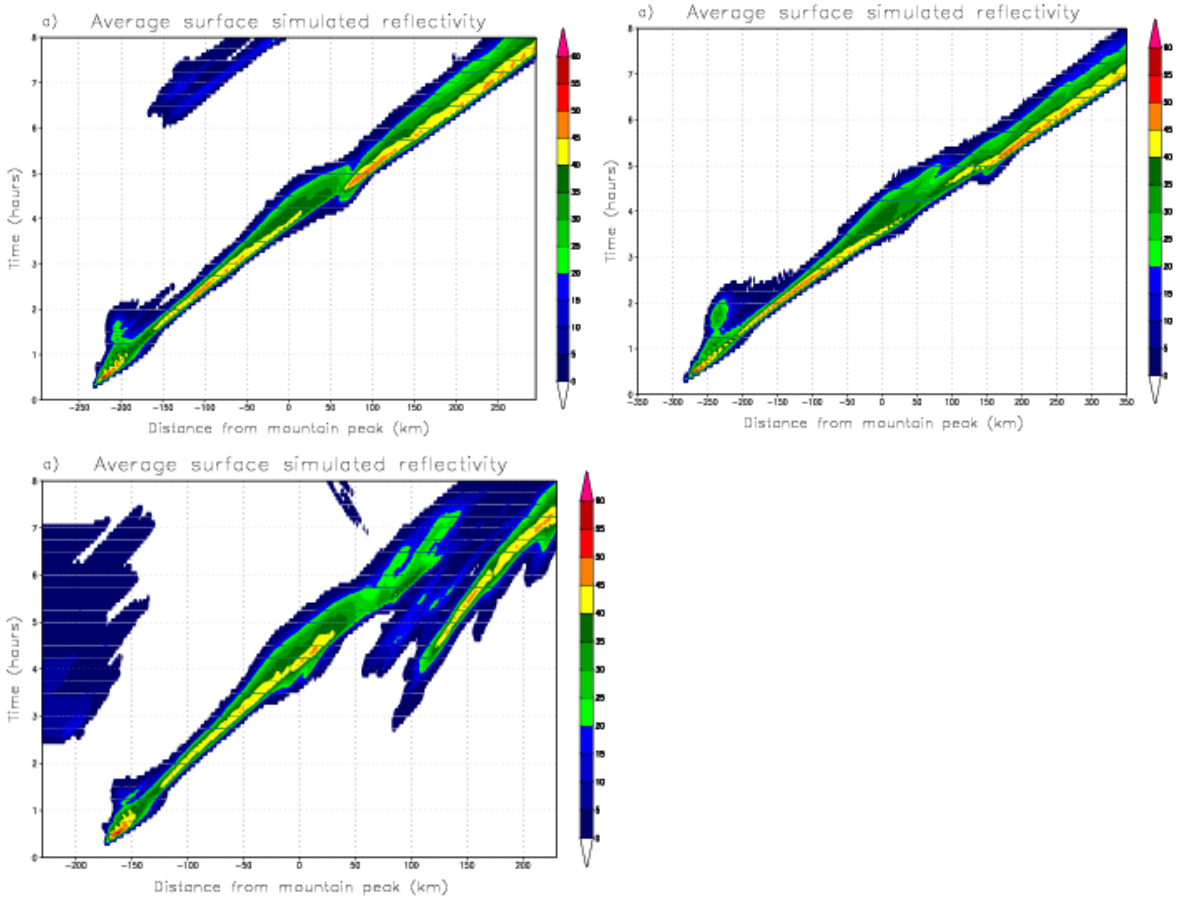

Figure 2.1: Hovmöller diagrams of the average surface simulated reflectivity for (a) the control wind profile simulation, (b) the increased mean wind +5 m/s simulation, (c) for the decreased mean wind -5 m/s simulation

Despite these impacts of the wind profile, each system was able to successfully cross the mountain as a result of a hydraulic jump in the outflow (as shown by Frame and Markowski 2006; Fig. 2.4) as the system descended the barrier as well as an environmental hydraulic jump (Figure 2.5) in the presence of sufficient flow over the terrain. The wave train resulting from the environmental hydraulic jump first produced new convective cells ahead of the system which quickly merged with the squall line and

then significantly reinvigorated the updrafts as the system encountered the lee wave train. Thus, despite greater suppression observed as the mean wind was increased, a more lee environmental hydraulic jump in addition to the hydraulic jump in the outflow resulted in the reintensification of updrafts downstream of the mountain. Additionally, the idealized simulations contained a favorable base-state thermodynamic environment with ample instability and minimal inhibition. As a result, parcels were easily lifted to their LFC and were able to tap into a significant amount of instability to produce vigorous convection once the hydraulic jump occurred and the lee wave train was encountered.

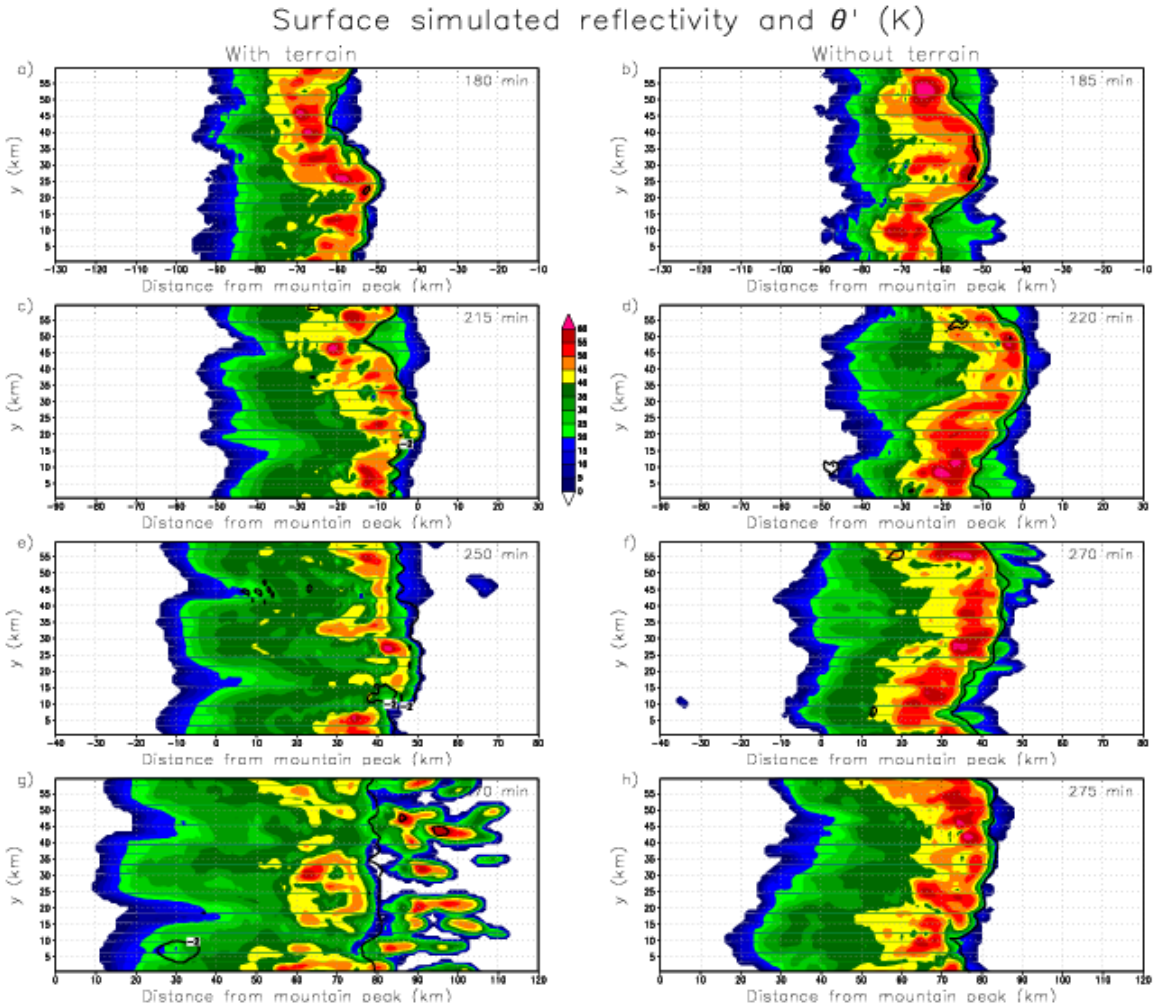

Figure 2.2: Plan views of surface simulated reflectivity depicting the evolution of the MCS over time (as noted on each panel) for the increased shear +5 m/s simulation with (left) and without (right) terrain. The thick black contour outlines the leading edge of the cold pool (where θ'= -2 K)

From the initial modeling study, we conclude that while the wind profile can modulate the crossing process, primarily through stronger or weaker slope flows, given a favorable thermodynamic environment, an MCS will be able to traverse a barrier. An additional set of simulations tested a variety of less favorable lee thermodynamic environments. Nearly

all simulations still produced crossers; however, when both lee cooling and drying was present, along with a stronger mean wind, a noncrosser was produced (see attached figures in email). Therefore, while the presence of sufficient downstream instability and minimal inhibition primarily influences crossing potential, modifications to the wind profile have more influence on crossing ability when the lee thermodynamic environment is less favorable. Overall, forecasters are encouraged to first and foremost consider the amount of downstream instability and inhibition, but also to keep in mind the impacts of the wind profile when trying to forecast the maintenance of an MCS approaching the Appalachian Mountains.

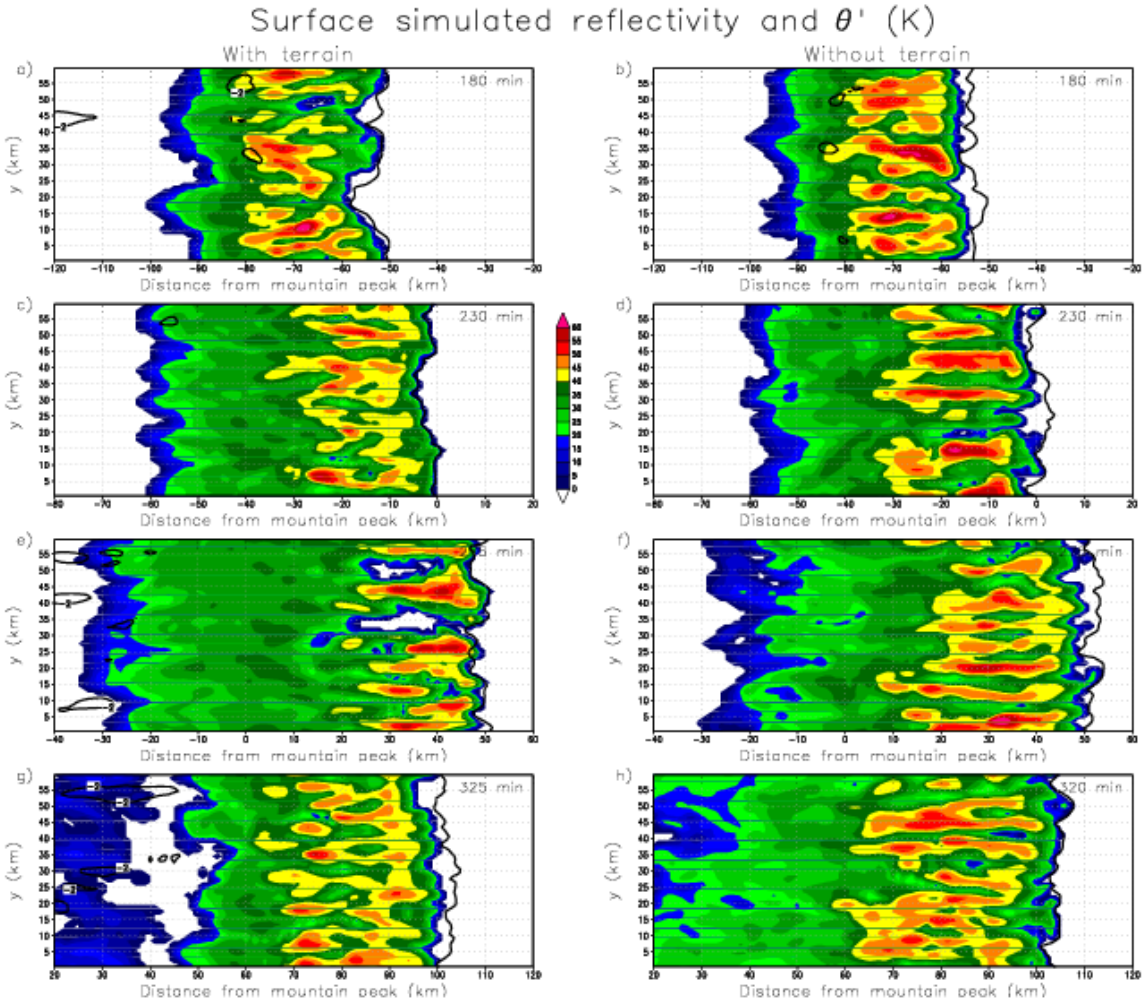

Figure 2.3: As in Figure 2.2, but for the decreased shear -5 m/s simulation

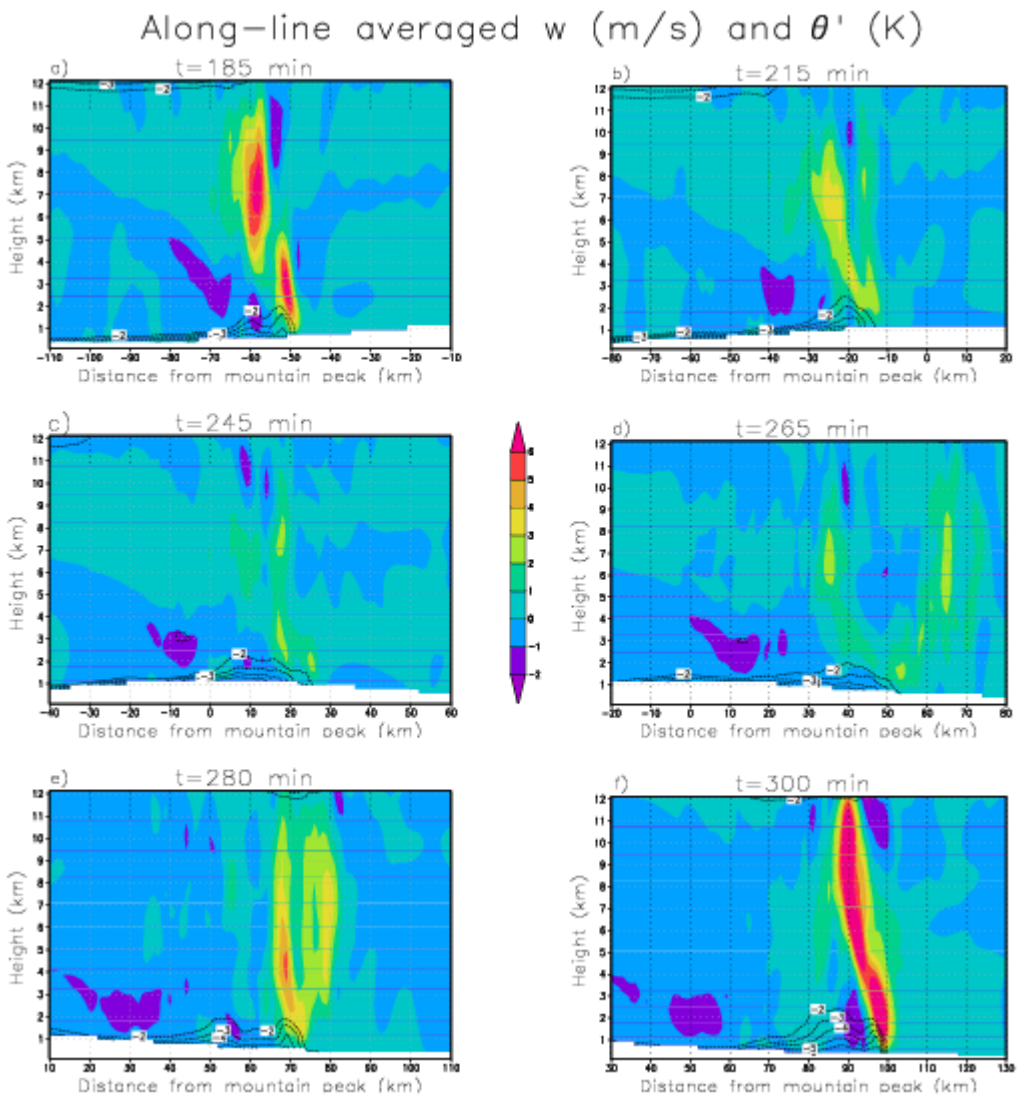

Figure 2.4: Along-line averaged vertical cross sections of vertical velocity (shaded) and θ’ (contoured) over time (as noted on each panel) for the control simulation with terrain

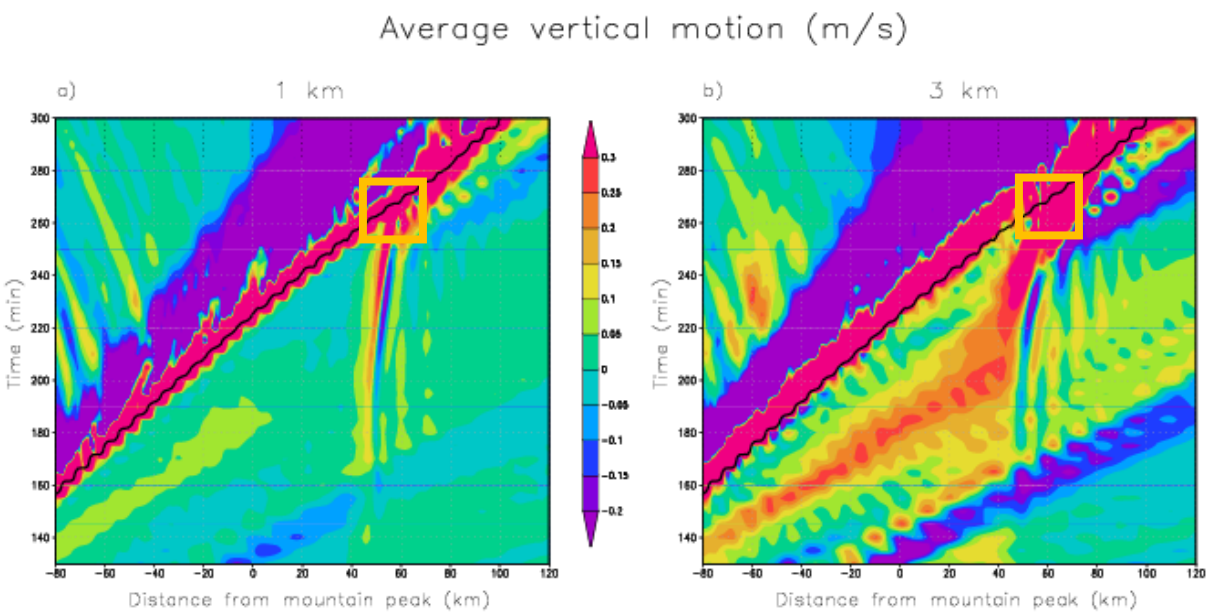

Figure 2.5: Hovmöller diagrams of the averaged vertical velocity for the control simulation with terrain at a) 1 km and b) 3 km. The thick black line denotes the position of the outflow boundary as indicated by the θ'= -2 K contour. The orange box indicates the time and location in which the system underwent the strongest reinvigoration.

Casey defended her M.S. thesis on 24 April 2009, and since that time has published two articles, one in *Weather and Forecasting* and one in *Monthly Weather Review*, presenting these results (Letkewicz and Parker 2010, 2011). Concerning presentations, in addition to the aforementioned NWS site visits, she presented her work during the 28 October 2010 CSTAR meeting in Raleigh. Some further developments include the exploration of additional observational avenues. These include examining how the environment *changes* from upstream to downstream of the mountains on a case-by-case basis, analyzing radar data to look at fine lines and other radar signatures to assess whether cold pools can be clearly seen to cross the barrier, construction of composite surface and 500 hPa maps, and further statistical analysis of the discriminatory power of various wind components (including mountain-perpendicular, mountain-parallel, north-south and east-west). The results of these further activities did not change the overall key message of the study, but enhanced the existing results. For example, the cross-barrier difference calculations showed that crossing cases not only occur in environments with higher CAPE, but also they move into lee environments that have *more* instability than the windward environment. Examination of the radar signatures was inconclusive, owing largely to the horizontal and vertical limitations of radar coverage in the Appalachians. The composite charts showed few large-scale differences at 500 hPa, and a few more noticeable differences at the surface, but overall they suggest that pattern recognition is not particularly useful in separating crossers from non-crossers. Although individual wind components were not statistically discriminatory, we found that many of the crossing cases occur under south to southwesterly surface flow in the lee, which has potential relationships to both instability and vertical wind shear in the lee.

In distilling all of the observational evidence, we provide the following "final recommendation" to forecasters. Instead of emphasizing lee SBCAPE as the most discriminatory parameter, we instead recommended the use of lee MUCAPE (which is nearly as discriminatory), for two reasons. First of all, the accompanying MUCIN was more discriminatory than SBCIN, and its use combined with MUCAPE successfully delineates a majority of our cases (Figure 2.6). And secondly, MUCAPE is a more general requirement for convection (elevated convection is possible even when SBCAPE=0 J/kg). We continue to find that the downstream wind profile is also discriminatory, and is of particular influence when the thermodynamic environment is less favorable. In terms of operational utility, we first and foremost recommend investigation of MUCAPE and MUCIN in the lee when attempting to anticipate crossers vs. non-crossers.

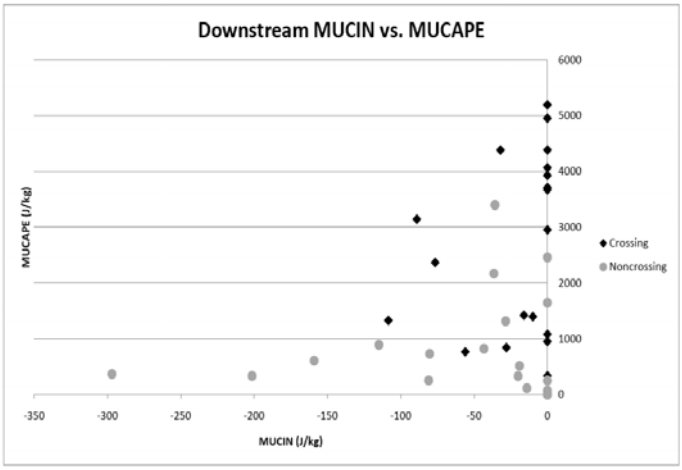

Fig. 2.6. Distribution of crossing (black diamond) and non-crossing (gray circle) MCS cases in terms of their environmental MUCAPE and MUCIN in the downstream (lee) sounding.

Letkewicz, C. E., and M. D. Parker, 2010: Forecasting the maintenance of mesoscale convective systems crossing the Appalachian Mountains. *Wea. Forecasting*, **25**, 1179-1195.

Letkewicz, C. E., and M. D. Parker, 2011: Impact of environmental variations on simulated squall lines interacting with terrain. *Mon. Wea. Rev.*, *in press.*

iii.) Tornadoes in landfalling tropical cyclones (Morin and Parker)

Graduate student Matt Morin used a "pseudo-idealized" version of the WRF-ARW model to study tornadic supercells embedded within the rainbands of a simulated hurricane. Based upon previous meetings with Scott Sharp of NWS-Raleigh and other NWS forecasters, Morin and Parker targeted the problem of relating observed radar signatures to actual physical processes within the supercells embedded in tropical cyclone (TC) rainbands. Based on further interactions with NWS collaborators, strong foci on the role of dry air intrusions and processes associated with tropical cyclone (TC) landfall were also emphasized in this work.

Matt Morin performed a series of computationally demanding, high-resolution numerical simulations that successfully captured embedded supercells in the TC environment. The reference experiment (i.e., the "control" run), hereafter referred to as "CTRL", features a hurricane heading due west over the open ocean. In this and the rest of the runs, tropical cyclone (TC) supercells form and evolve naturally within the rainbands of a creditable simulated TC. To address certain gaps in the TC supercell knowledge base, several variations of CTRL are used in this study as well, including runs where the TC makes landfall at different times of the day, runs with an artificial midlevel dry air intrusion, and runs with a combination of each.

The landfall simulations are used to, among other things, test the hypothesis that the sea-to-land transition is a crucial factor in TC supercell intensification due to the impacts of (1) a larger diurnal temperature variation, and (2) increased surface friction, which lengthens the hodograph in the TC's right-front quadrant (RFQ). Because this is a TC-supercell study, "landfall", for our purposes, is defined as the moment that isolated cells within the outer rainband first pass over the coastline. Preliminary results show that landfall time of day has a substantial impact on the average number, strength, and lifetime of simulated rotating storms embedded within the TC's rainbands.

The dry air intrusion simulations are used to test the hypotheses that storm-scale processes that lead to updraft rotation are enhanced in TC supercells that develop in and around dry air intrusions due to (1) midlevel evaporational cooling, which steepens the local lapse rate, and (2) cloud erosion, which leads to increased surface insolation and higher surface temperatures during the day. Recent work has gone into ensuring that the location for the area of artificial drying (the "dry box") in the simulations is realistic and allows the TC to effectively ingest the pool of dry air into its circulation. The research goal was for the midlevel dry air intrusion to reach the RFQ before outer rainband supercells start making landfall. After much experimenting, Matt has settled on a model configuration where the resultant RFQ relative humidity profile within the simulated dry air intrusion has remarkable similarities to those sampled in real observed cases.

The fourth (and finest) model domain is the primary source of data for this study and is launched during certain 10-hour periods. Domain 4 has a grid spacing of 667 m and covers a radial distance of ~775 km in the TC's RFQ. Figure 3.1 illustrates the structure of the simulated hurricane in this domain as well as its rainbands, where embedded supercells are identified and tracked (e.g., red lines in Figure 3.2). This study uses a set of

updraft-helicity-based metrics that enable us to compare the population of simulated supercells among the various simulations, allowing us to generate suitable statistics for testing our hypotheses (e.g., Table 3.1). Helical updrafts are determined by computing updraft helicity (Kain et al. 2008), which quantifies the degree to which strong updrafts and positive vertical vorticity are correlated. For each simulation, the finest mesh (Domain 4) is launched during four separate 10-hour windows. During each analysis window, the objective identification scheme is used to track supercells and record their fundamental parameters at a 5-minute interval. As of this progress report, final statistics for the objectively identified supercells are being compiled for each of the five primary simulations. The remaining work will then be directed toward physical explanations for the quantitative differences that emerge among runs in the days after a dry intrusion has been introduced (and/or landfall has occurred). Future work will involve compiling statistics for the objectively identified supercells for each of the five primary simulations and providing physical explanations for the quantitative differences that emerge among runs in the days after a dry intrusion has been introduced (and/or landfall has occurred).

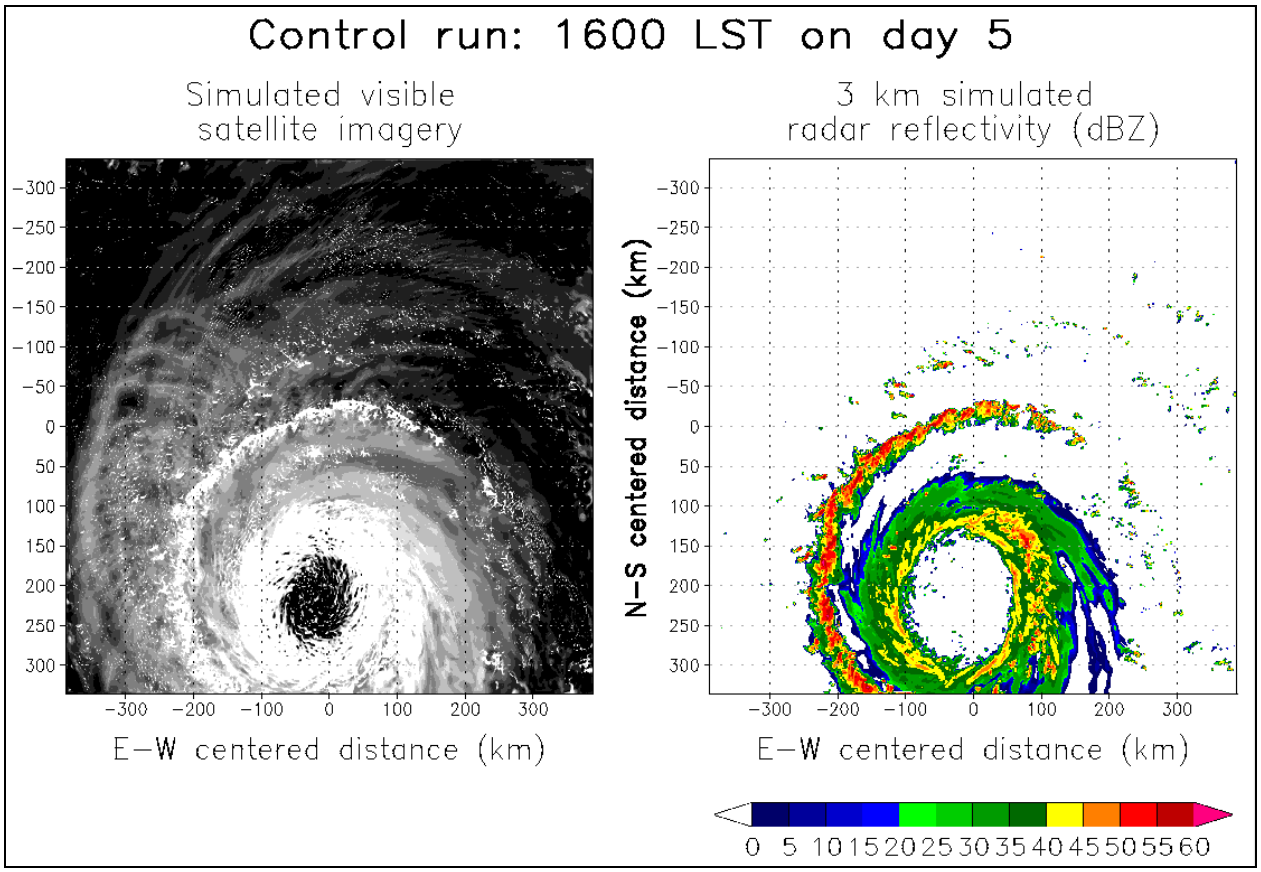

Fig. 3.1. Simulated visible satellite imagery (left) and 3 km simulated radar reflectivity (right) for the control run.

In addition to the aforementioned quasi-idealized simulations, if time permits, this study will also utilize "benchmark" simulations using a highly idealized version of the WRF model. These series of simulations will provide storm-scale analysis of a supercell

initiated by a warm bubble (as well as by convergence forcing) in a single sounding "TC-supercell" environment, which is taken from data in the finest grid of the full TC simulations. The purpose of these simplified benchmark runs, generally speaking, is to determine whether or not the hurricane itself needs to be simulated in order to produce realistic TC supercells. In other words, we are testing to what degree the variability in the hurricane matters. For real TC supercells, there is a lot of mesoscale variability in the wind and thermodynamic fields, which is driven by the rainbands and parent TC circulation. If the supercell in the benchmark simulation fails to evolve, or fails to resemble real TC supercells, then the homogeneous sounding concept for simulations will be undermined. If the two are similar, then we can show that the local ingredients are more important to the supercell than the parent storm's macro-scale circulation.

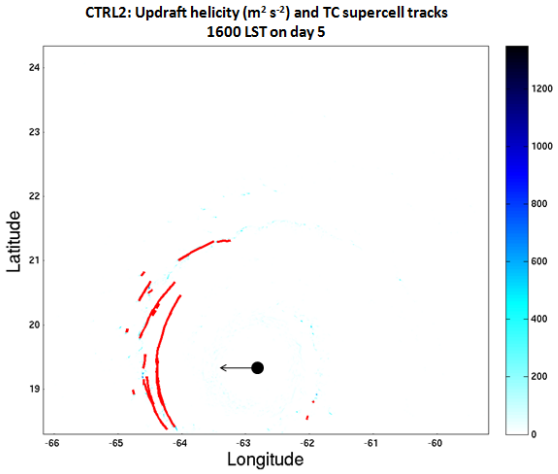

Fig. 3.2. Tracks of cells that surpass the updraft helicity threshold of 675 m^2 s^{-2} in the control simulation. The black dot represents the estimated location of the TC eye, while the arrow denotes the direction of TC motion. Figure 1 provides a clearer picture of the location and structure of the rainband responsible for generating these particular rotating storms.

Following his successful thesis defense, Matt published a manuscript in *Geophysical Research Letters* (GRL) presenting this work. Based on feedback from his thesis defense, Matt configured a new model experimental design that improves upon the original, as discussed below. The new series of simulations feature more realistic initial conditions and model settings. For example, domain 1 is now centered at 20°N, rather than at the equator[1] (top of Fig. 3.3). In both situations, the model is still run on a 20°N *f*-plane. However, with the 'XLAT' variables in WRF representing a domain centered at 20°N, there is a more realistic distribution of downward shortwave radiation values over the domain (bottom of Fig. 1). In addition, a more appropriate initial value for soil and surface skin temperature is specified. Originally, the upper soil levels were too cold at the beginning of the simulation (though they evolved naturally over time and the diurnal

[1] The original placement of the domain allowed for a larger size without running into memory issues on the computer system used at the time.

temperature shifts equilibrated with the environment well before outer rainband landfall). Phase 2 simulations have initial soil (all layers) and surface skin temperature set to 295 K (rather than the former setting of ~285 K).

Time	Run	Number of tracks	Max lifetime (minutes)	Avg lifetime (minutes)	Median lifetime (minutes)	Max UH ($m^2 s^{-2}$)	Avg UH ($m^2 s^{-2}$)	Median UH ($m^2 s^{-2}$)
Day 5: 12-2000 LST	CTRL	384	160.00	14.96	5.00	3760.30	1113.70	934.41
	DLAND	266	130.00	15.43	10.00	2554.00	975.97	858.55
	NLAND	---	---	---	---	---	---	---
	DAI_CTRL	418	105.00	11.39	5.00	3077.60	1025.40	909.40
	DAI_DLAND	259	125.00	17.84	10.00	3186.00	1025.20	902.40
Day 6: 00-1000 LST	CTRL	546	180.00	13.28	5.00	4328.40	1252.90	1099.40
	DLAND	45	55.00	12.00	10.00	2535.30	865.77	791.03
	NLAND	199	70.00	12.04	5.00	2648.20	947.97	864.06
Day 6: 12-2000 LST	CTRL	537	255.00	13.45	5.00	5461.30	1136.70	968.25
	DLAND	112	145.00	15.63	7.50	2584.10	922.10	830.16
	NLAND	37	100.00	11.76	5.00	1676.00	884.65	792.57
	DAI_CTRL	491	265.00	15.18	5.00	4218.30	1219.70	1032.40
	DAI_DLAND	216	190.00	14.72	10.00	2257.70	955.12	862.90
Day 7: 00-1000 LST	CTRL	---	---	---	---	---	---	---
	DLAND	10	30.00	12.00	10.00	1504.70	902.21	774.95
	NLAND	236	105.00	12.73	5.00	2311.00	880.75	809.84

Table 3.1. Example of statistical output from the "blob" detection/tracking algorithm for each of the model runs used in this study (where data are currently available).

For the new landfall simulations, the coast is positioned at a specific longitude, such that outer rainband landfall occurs at 15 UTC (12 LST). If the model is restarted at 12 UTC (00 UTC) on the day (night) of landfall, and spin-up time of 1 hr is allocated for domain 4, then there are 2 hrs of pre-landfall supercell analysis. It will be important to show that, during the 2 hrs before landfall, supercell activity is minimal (and actually may decrease over time during the day[2]), and it is only when the rainband moves over land that supercell activity first increases significantly. Since the TC slows down somewhat as it approaches the coast, it took Matt a few attempts to set up a true "daytime" landfall simulation. Serendipitously, he now has "morning" and "evening" landfall runs for potential future use (the SOO at the Raleigh weather forecast office has also expressed an interest in seeing resultant supercell behavior in these data).

[2] The thermally direct circulation and onshore convection that occurs during the day drives subsidence offshore out to ~1000 km. At night, this effect diminishes and TC supercells are no longer inhibited near-offshore.

Another change from the old model configuration is the implementation of a surface roughness modification following Nolan et al. (2009). The problem with the original formulation was that, for increasing surface wind speed, there are steadily increasing values of surface roughness length, which also drive increasing values of the surface drag coefficient. From observations, the surface drag coefficient in high winds levels off for wind speeds > 30 m s^{-1}. The surface roughness modification was designed to prevent resultant run-away surface fluxes within the TC environment, which in turn reduced TC intensity. With TC intensity reduced, Morin and Parker decided not to apply the previously used Smagorinsky modification to the current simulations. With the horizontal mixing length term allowed to scale with horizontal grid spacing, the model was less diffuse and convection was better resolved on the 2 km grid. Furthermore, the increased detail of convection in domain 3 allowed for a faster "spin-up" time for domain 4 when it was launched, which means there is more time for high-resolution analysis of offshore supercells before the outer rainband makes landfall.

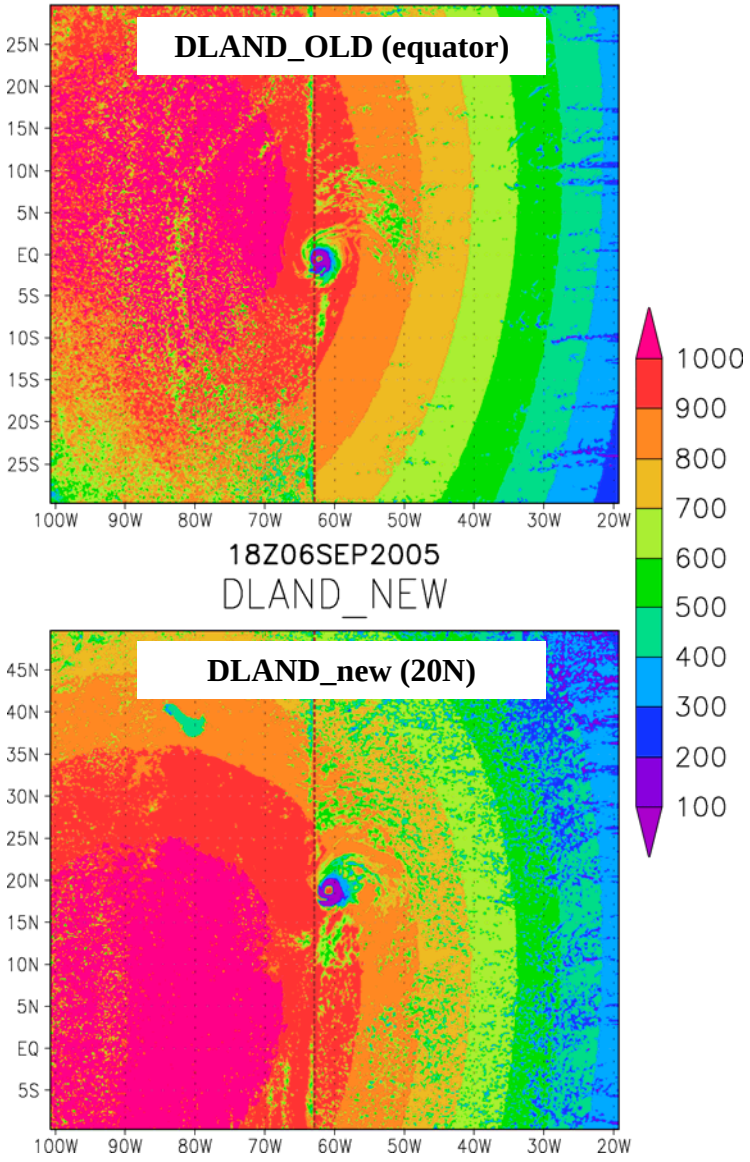

Figure 3.3: Downward shortwave radiation (SWDOWN; W m^{-2}) for the (top) thesis and (bottom) new versions of DLAND. Land is west of the brown dashed line.

In Part II of Nolan et al. (2009), it is stated that, "Even with these improvements [i.e., the surface roughness modification], the MYJ consistently produces larger frictional tendencies in the boundary layer than the YSU scheme, leading to a stronger low-level inflow and a stronger azimuthal wind maximum at the top of the boundary layer." It is still not entirely clear which of these PBL schemes is most "accurate". The MYJ scheme tends to mix a shallower boundary layer over land during the day in the TC supercell environment, which leads to greater 0-3-km SRH (for TCs with similar intensities) and greater SBCAPE than in the YSU simulations (e.g., SBCAPE values in Fig. 3.4). DLAND simulations using the YSU configurations end up with a weaker TC, which has a substantial impact on the overall wind profile. For fair comparison with MYJ, a DLAND simulation with SST=27°C (a 1° increase) was run (Fig. 3.4, left side and red lines in sounding diagram), such that TC intensities would be similar between the runs at the time of landfall (minimum SLP in the YSU run actually ended up ~5-10 hPa lower than MYJ during landfall). Results show that the increased SST was indeed beneficial to enhancing the wind profile in the TC supercell environment (Fig. 3.4). For similar TC intensities, the 0-1-km wind field via the YSU scheme actually has SRH similar to observed TCs. Therefore (and since it is evident that the YSU resultant thermodynamic profile is typically more realistic than MYJ), the YSU PBL scheme along with 27°C SSTs will be used subsequently. This decision is further supported by the default use of this scheme in WRF's (V3.3) new test case "em_tropical_cyclone", as well as by the inclusion of new TC-specific namelist options available specifically for the YSU scheme in WRF (V3+).

Lastly, suspecting the ambient TC environment may still be unrealistically/unfavorably dry, Matt made a slight modification to the initial moisture profile, where relative humidity is constant at 80% from the surface up to 500 hPa, and then tapers off to 50% as before (Fig. 3.5). Since finalizing his thesis results, the question still remains as to what led to more (and longer-lived) supercells in the dry-air intrusion (DAI_DLAND) experiments compared to DLAND. Conventional (e.g., sounding) analyses did not reveal a significant difference in the temperature profiles within the supercell environments among the runs. A moister environment (with more cloud and stratiform rain cover) may make any differences more obvious and/or the answer may lie in potential instability analyses. Nevertheless, Matt has worked to finalize the next series of DAI simulations, as well as the "Benchmark" runs after the final "full-TC" model configurations are tested.

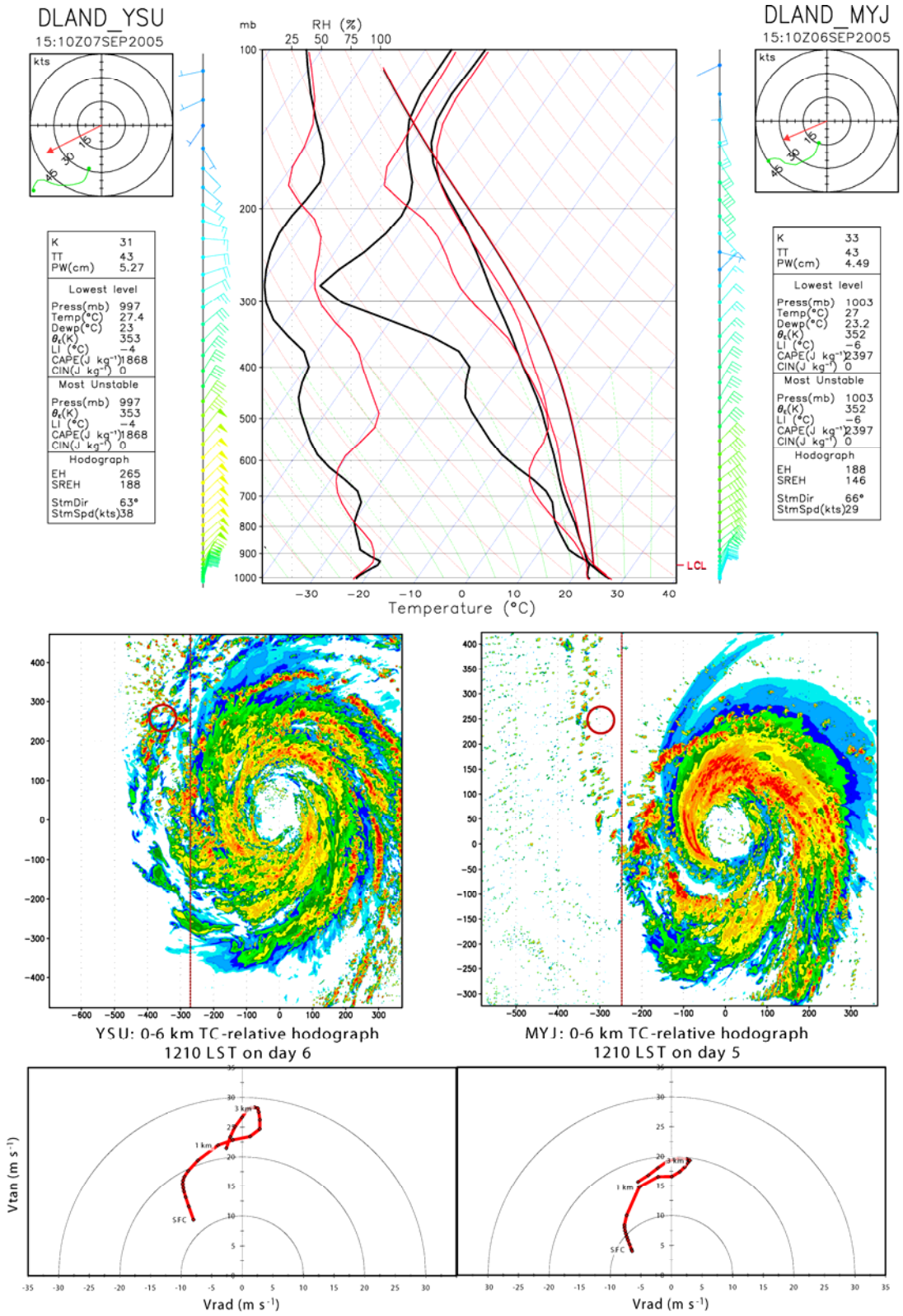

Figure 3.4: Comparison of TC supercell environments for (left; red traces in sounding) DLAND_YSU and (right; black traces in sounding) DLAND_MYJ. TC intensity slightly higher in DLAND_YSU (min. SLP is ~7 hPa lower).

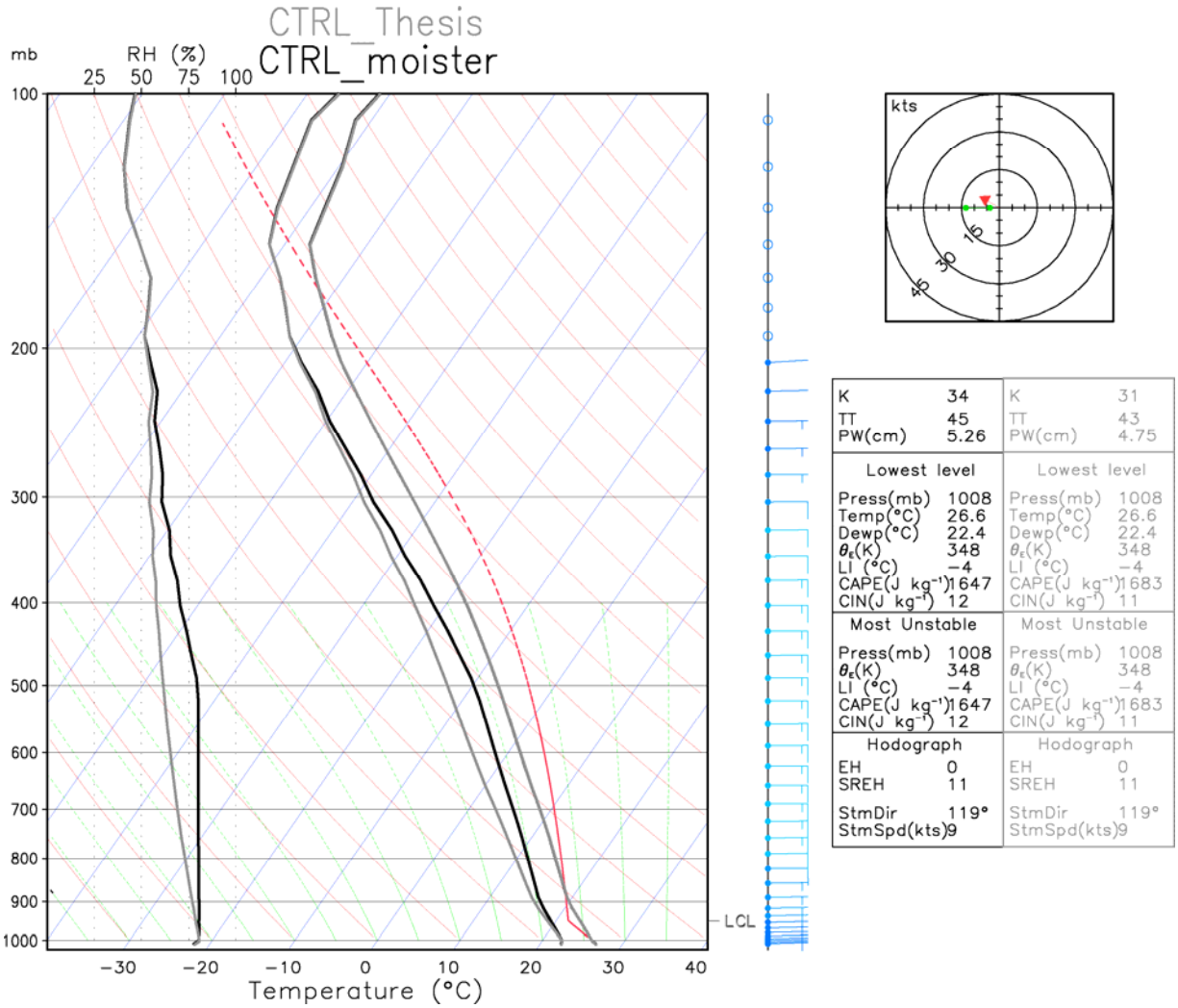

Figure 3.5: Skew-*T* ln-*p* diagram for the initial soundings of the thesis (gray traces) and new (black traces) version of CTRL. Temperature profiles are unchanged, and the red dashed line shows the approximate CAPE profile, which was only slightly changed due to the increased moisture in the environment.

The following is a summary of operationally relevant lessons from this research:

- Landfall is found not to be necessary for supercell development in our simulations. The optimal ingredients for our simulated supercells are found over the open ocean However, in the real world: (i) upwelling causes decreasing SSTs (decreasing CAPE), and (ii) approaching land can weaken the TC, decreasing shear. For TC-tornadogenesis, however, the effects of landfall (and land in general) are most likely still needed to tilt, converge, and stretch the supercell's baroclinically generated low-level vorticity.

- SBCAPE is indeed enhanced over land during the day due to surface insolation, making the onshore thermodynamic environment in a landfalling TC more favorable for supercells compared to offshore

- Within the RFQ in a landfalling TC, supercell development is favored by the enhanced low-level SRH onshore compared to offshore. Increased surface friction over land slows and backs the 0-500 m winds

- A nocturnal landfall was associated with much fewer and shorter qualifying supercell tracks than DLAND's landfall. However, the supercell environment during a nocturnal landfall can still locally provide the necessary instability for the development of supercells within a narrow corridor along the coast.

Caveat: This may be applicable for real nocturnal landfall environments where there are no external boundary interactions to initiate convection. Also, for North Carolina nocturnal landfalls, I suspect that TC development would be favored offshore due to the presence of the warm Gulf Stream. Recall that during the night, there is no near-offshore subsidence, which would normally inhibit (to some degree) convection.

TAKE HOME MESSAGE: The inland supercell threat is greatest overall during an afternoon landfall. However, nocturnal supercells do move ashore in our simulations and the threat continues into the next day.

iv.) Flooding research and TC QPF and modeling (Tang and Xie)

The overarching goal of this component of the project is to improve understanding of meteorological and hydrological processes during landfalling tropical cyclones. The development of this understanding necessitated the adapting a watershed model to the Tar-Pamlico Watershed in central and eastern North Carolina. The model of choice was the USDA AGNPS model, as this model was well-tested in other watersheds and also contains a water quality component which can be used to study the ecological impacts of inland flooding. To port the model for the Tar Pamlico watershed, ground water, soil, land use and meteorological data were be collected and integrated into the model.

For use during a tropical cyclone, additional adaptations were needed in the model. A focus on ground water recharge, and the including of channel routing were needed to allow accurate simulation of runoff and flooding processes during the example case of Hurricane Floyd (1999). Regarding the hydrological aspect, we have answered questions such as:

1) How do tropical cyclones interact with coastal watersheds?
2) Why do some of tropical cyclones cause more flooding than others even when the storm characteristics are similar?
3) What role does soil moisture content play in the flooding?
4) How quickly does the peak discharge react to rainfall in the Tar Pamlico river basin?

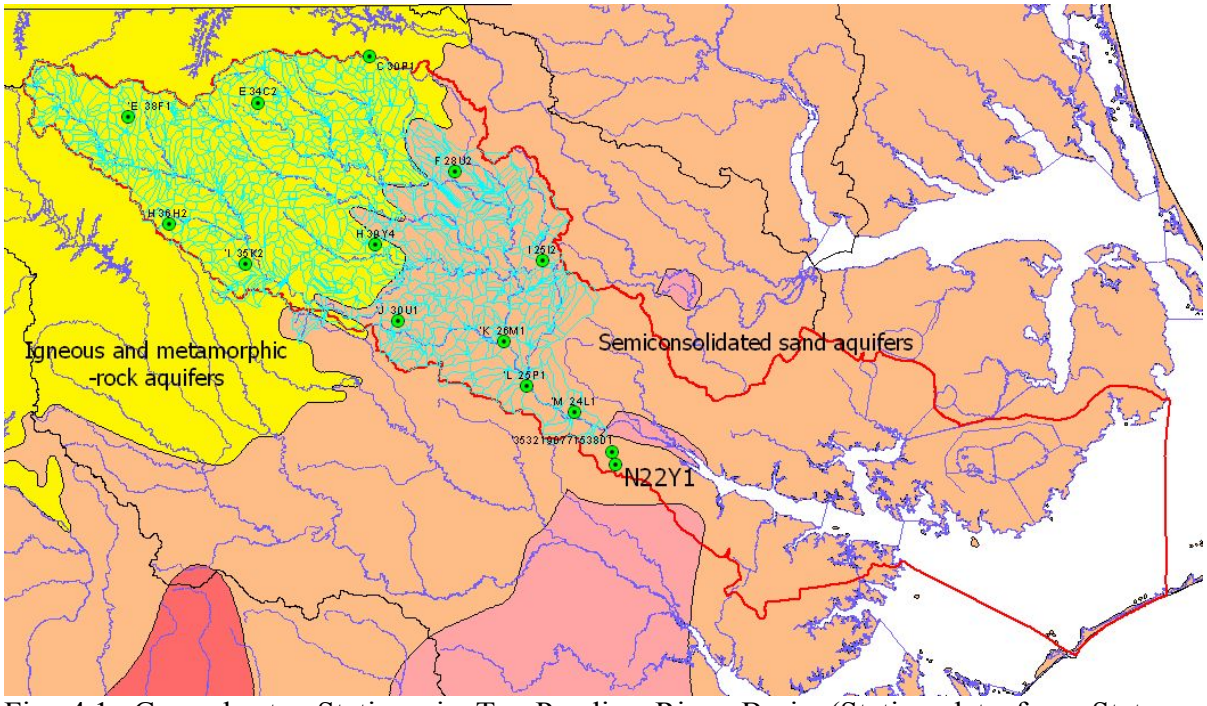

Fig. 4.1. Groundwater Stations in Tar Pamlico River Basin (Station data from State Climate Office)

Hurricane Floyd produced large amounts of precipitation, on top of that, soil moisture content and ground water level were both very high before the arrival of Hurricane Floyd

due to the previous landfall of Hurricane Dennis. According to historical groundwater records, groundwater level at station N22Y1 at lower Tar Pamlico near the outlet of the watershed (Fig. 4.1) is merely 0.05 meters below the surface on Sept. 10, 1999. This is just 5 days before Hurricane Floyd's landfall at 0630 UTC on Sept. 16, 1999. In other words, at the outlet of Tar Pamlico River Basin before Hurricane Floyd landfall, the ground water recharge in the runoff almost reached the surface. Thus, any additional precipitation after Dennis would likely cause flooding. This working hypothesis was tested, with results summarized below.

Tropical cyclone QPF and modeling

A second focus of the work of Q. Tang involved analysis of precipitation during hurricane Floyd derived from WRF simulations of Hurricane Floyd. Figure 4.2 is a schematic map of interactions between the atmospheric environment, landfalling hurricanes, and previous rainfall events with a watershed hydrological response during hurricane landfall. Storm surge induced by strong hurricane wind is not included in this research.

Table 4.1 is the comparison of WRF-simulated precipitation and observations. Due to the observation time at 7 or 8 am for most cooperative observer stations, the WRF model output from the corresponding time is used for comparison. Observations at 12 o'clock midnight local time are not included in the comparison. Except for the station at Scotland Neck No 2, the difference between the simulated and the observed precipitations is less than 30% of the observed values. Five out of 13 simulated station precipitation totals are within 10% of the observed values. The distributed precipitation output data from the WRF model (see Fig. 4.3 and 4.4) were then utilized as input into the AnnGNPS model to simulate the total runoff (Fig. 4.5).

The Hurricane Floyd event was accompanied by significant synoptic-scale forcing for ascent. To what extent was the heavy rain due to synoptic forcing as opposed to the tropical system? Of course, the synoptic environment is altered by the presence of Floyd, and so it is difficult to truly separate these factors. However, in a sensitivity study, the atmospheric environment-induced precipitation was analyzed by removing tropical cyclone vortex before hurricane landfall. The results are shown in Fig. 4.6. The environment-induced precipitation is mostly distributed in eastern NC. In the study area, there is only a small amount of environmental precipitation in the no-TC simulation. Table 4.2 presents the environmental (non-TC) precipitation at the observation stations. The results suggest that in general, <10% of the total event precipitation is induced by synoptic-scale environment in the study area.

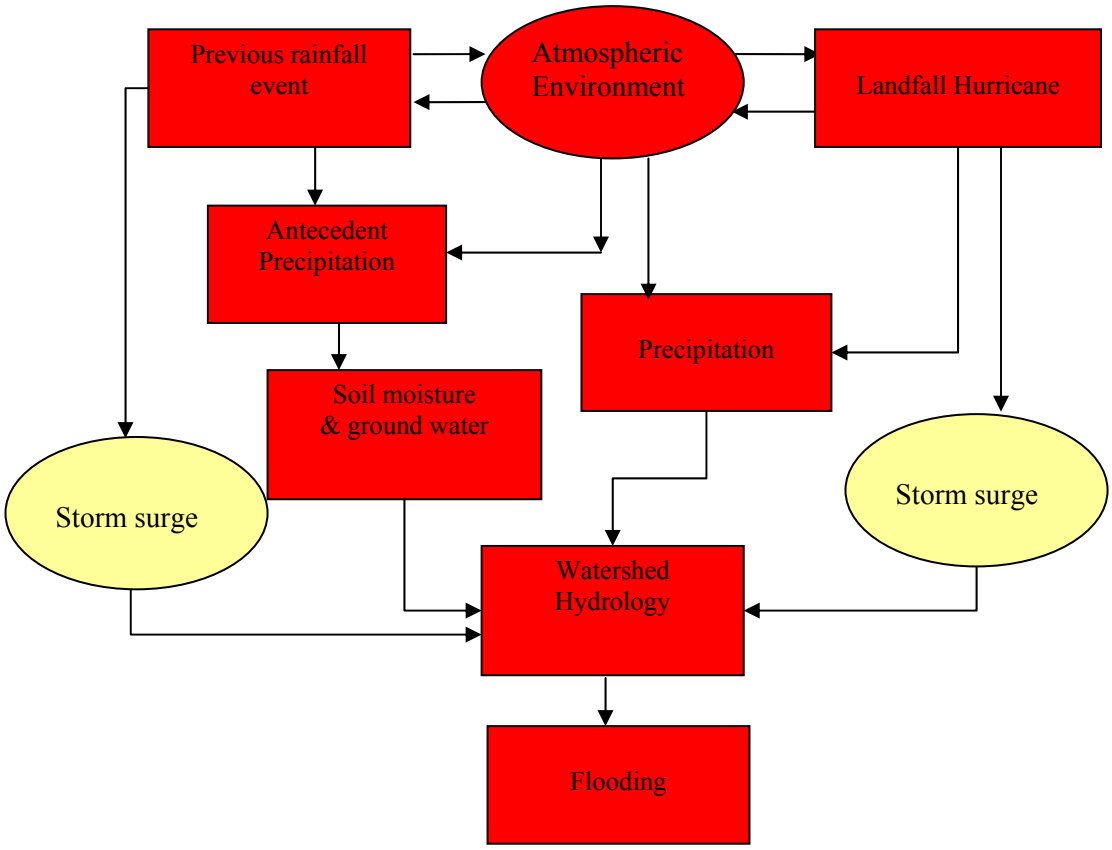

Fig. 4.2. Schematic interaction map of antecedent precipitation, atmospheric environment and landfalling tropical cyclone-induced precipitation, watershed hydrological response and storm surges. The yellow boxes are phenomena not studied in this research.

In summary, this proof-of-concept study demonstrated the viability of using numerical model QPF to drive a properly configured hydrological model. Once channel routing and ground water were properly accounted for, the hydrological model was able to accurately represent the observed flooding event. In the future, output from a model such as WRF could be used to drive a hydrological model in real time.

Analysis of the rainfall during Floyd demonstrates that the presence of the TC, and its interaction with an environment featuring an upper-level trough and jet entrance region was critical to the heavy rainfall. This was strongly suspected based on the results of earlier studies (e.g., Atallah and Bosart 2003; Colle 2003), but the experimental design employed here allowed confirmation and quantification of this fact.

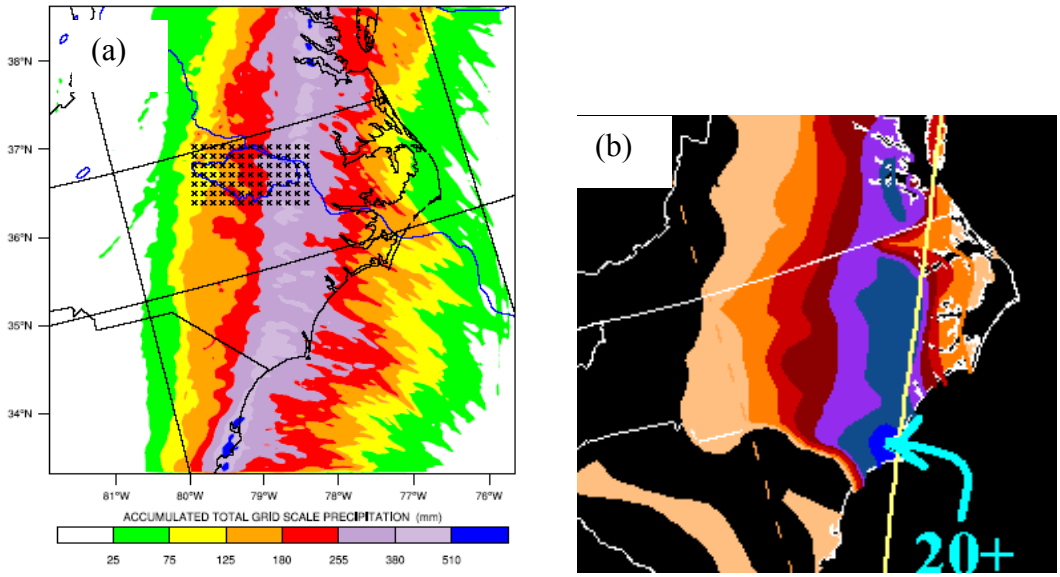

Fig. 4.3. Accumulated precipitation from (a) WRF model (b) Observations (NOAA) during Hurricane Floyd landfall from 1200 UTC Sep 15 – 1200 UTC Sep 17, 1999 (blue crosses are points used to get WRF information for hydrological model precipitation input, line under cross point are research area). In panel (b), blue is 510mm; dark blue is 380mm; violet is 255mm; dark red is 180 mm; red is 125mm; orange is 75mm and yellow is 25mm (NOAA).

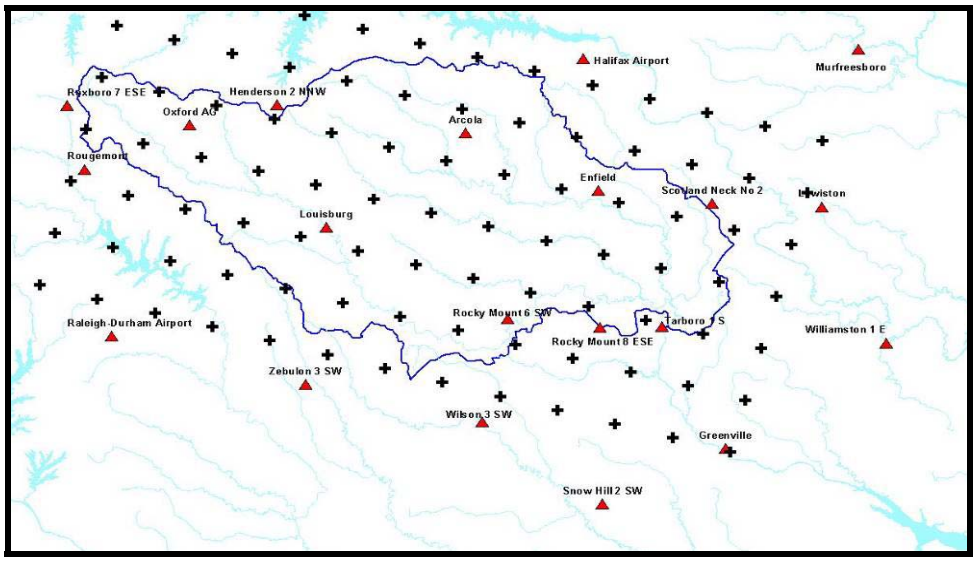

Fig. 4.4 AnnAGNPS model input precipitation points from WRF model output (Black cross, red triangle points represent the location of rainfall observation stations).

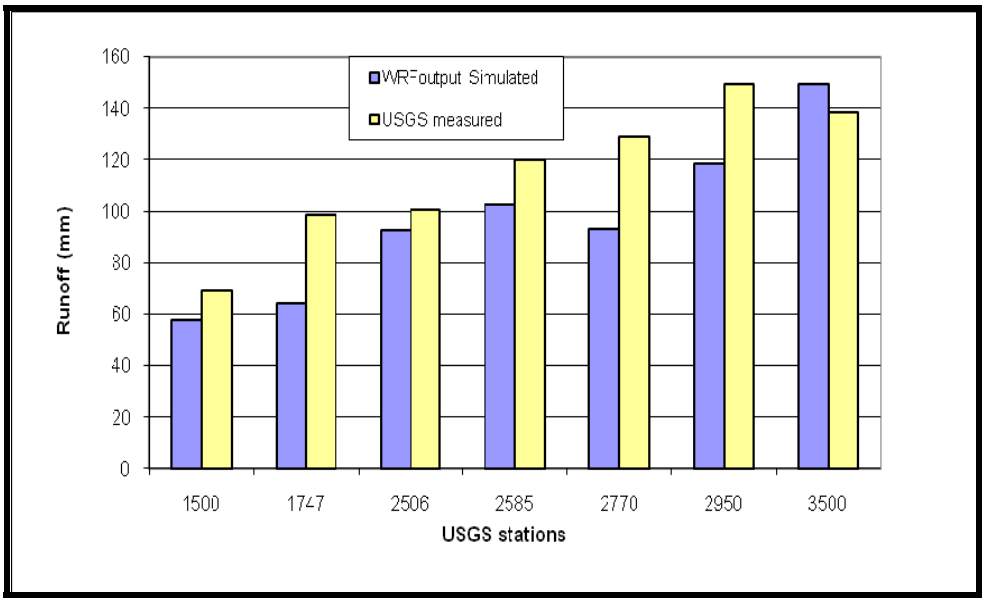

Fig. 4.5 Comparison of WRF output simulated runoff and USGS observed runoff at seven watersheds.

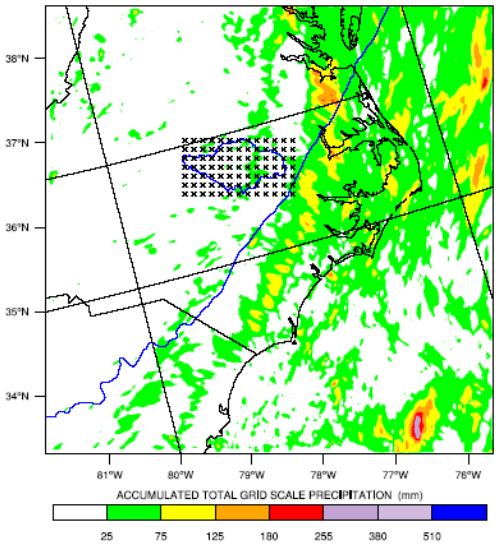

Fig. 4.6 Accumulated precipitation after removing Floyd from the model initial conditions (blue polygon is study area and blue line is pressure contour).

Table 4.1 Comparison of WRF simulated with observed total precipitation during Floyd landfall in NC

Station Name	Station ID	Latitude	Longitude	Observed Total Precipitation (mm) on Sept 16 and 17, 1999	Simulated Total Precipitation (mm) Sept 16 and 17, 1999			Differences in Percentage (Simulated – observed)		
					Domain 1	Domain 2	Domain3	Domain1	Domain 2	Domain 3
Arcola	310241	36.29	-77.98	224	225	244	251	1	9	12
Enfield	312827	36.17	-77.68	259	310	321	323	20	24	25
Greenville	313638	35.64	-77.40	314	318	307	312	1	-2	-1
Henderson 2 NNW	313969	36.35	-78.41	134	143	152	154	7	14	15
Louisburg	315123	36.10	-78.30	204	161	162	161	-22	-21	-21
Oxford AG	316510	36.31	-78.61	138	125	116	117	-10	-16	-15
Roxboro 7 ESE	317516	36.35	-78.89	123	92	90	91	-25	-27	-26
Rougemont	317499	36.22	-78.85	115	92	98	96	-20	-15	-16
Snow Hill 2 SW	318060	35.53	-77.68	387	385	404	386	-1	5	0
Scotland Neck No 2	317725	36.14	-77.42	277	377	407	409	36	47	48
Williamston 1 E	319440	35.85	-77.03	326	292	308	308	-11	-6	-6
Wilson 3 SW	319476	35.70	-77.95	259	253	284	300	-2	10	16
Zebulon 3 SW	319923	35.78	-78.35	237	175	178	189	-26	-25	-20

Table 4.2 Atmospheric environmental induced precipitation during Floyd landfall in NC

Station Name	Station ID	Observed Total Precipitation (mm) on Sept 16 and 17, 1999	Simulated Total Precipitation (mm) Sept 16 and 17, 1999			Simulated environmental precipitation (mm)			Environmental Precipitation Percentage		
			Domain1	Domain2	Domain3	Domain1	Domain2	Domain3	Domain1	Domain2	Domain3
Arcola	310241	224	225	244	251	11	8	8	5.00	3.24	3.38
Enfield	312827	259	310	321	323	21	16	14	6.63	5.05	4.19
Greenville	313638	314	318	307	312	29	54	34	9.04	17.63	10.79
Henderson 2 NNW	313969	134	143	152	154	15	5	3	10.55	3.32	1.76
Louisburg	315123	204	161	162	161	11	4	5	6.74	2.61	2.92
Oxford AG	316510	138	125	116	117	13	16	10	10.74	13.72	8.47
Roxboro 7 ESE	317516	123	92	90	91	3	2	4	2.72	2.55	3.91
Rougemont	317499	115	92	98	96	3	5	5	2.72	5.24	5.64
Snow Hill 2 SW	318060	387	385	404	386	21	16	22	5.41	4.03	5.57
Scotland Neck No 2	317725	277	377	407	409	14	23	24	3.63	5.68	5.92
Williamston 1 E	319440	326	292	308	308	57	55	55	19.72	17.95	17.88
Wilson 3 SW	319476	259	253	284	300	17	8	4	6.84	2.66	1.17
Zebulon 3 SW	319923	237	175	178	189	14	20	25	7.88	11.25	13.29
Average		**231**	**227**	**236**	**238**	**18**	**18**	**16**	**7.51**	**7.30**	**6.53**

Other work on warm season QPF

NWS Raleigh forecaster Barrett Smith has conducted simulations of Tropical Storm Hanna (2008) in order to better understand the role of a boundary feature in focusing the heavy precipitation across North Carolina in that event. These efforts are followed up in a subsequent CSTAR project.

Human Resources Development

M.S. student Adam Baker defended his thesis on 17 July 2009, and began work as a NWS employee at the Indianapolis, IN forecast office in December, 2009. Adam presented his CSTAR research at the National Weather Association 14th Annual Severe Storms and Doppler Radar Conference, Des Moines, IA, 27 March 2010, delivered four seminars, and developed a recorded online presentation of his findings.

M.S. student Casey Letkewicz defended her M.S. thesis on 24 April 2009 and is currently working with Dr. Parker as a Ph.D. student. Casey presented her work during the 28 October 2010 CSTAR meeting. Additionally, the first publication resulting from her CSTAR work is now in print in *Weather and Forecasting* (Letkewicz and Parker 2010), and a second paper in *Monthly Weather Review*, is now in press (Letkewicz and Parker 2011). Casey presented her work in two journal articles, made two site visits, and recorded a presentation of her findings.

Ph.D. student Qianhong Tang defended her dissertation on 27 July 2010; the topic of her project was flooding and tropical cyclone precipitation. Since her thesis defense, Qianhong has returned to China, where she works for the Chinese weather service.

M.S. student Matt Morin defended his thesis on 7 January 2011, and has completed his masters thesis. His work is focused on the problem of tornadoes spawned by landfalling TCs. Matt recorded an online presentation of his work, published results in *Geophysical Research Letters* (Morin and Parker 2011), and delivered two seminars presenting his findings. He is currently seeking permanent employment.

References:

Atallah, E. H., L. F. Bosart, 2003: The Extratropical Transition and Precipitation Distribution of Hurricane Floyd (1999). *Mon. Wea. Rev.*, **131**, 1063–1081.

Baker, A. K., M. D. Parker, and M. D. Eastin, 2009: Environmental ingredients for supercells and tornadoes within Hurricane Ivan. *Wea. Forecasting*, **24**, 223–244.

Colle, Brian A., 2003: Numerical Simulations of the Extratropical Transition of Floyd (1999): Structural Evolution and Responsible Mechanisms for the Heavy Rainfall over the Northeast United States. *Mon. Wea. Rev.*, **131**, 2905–2926.

Baumer, O., Kenyon, P., Bettis, J., 1994. MUUF v2.14 User's Manual. USDA Natural Resource Conservation Service, Lincoln, Nebraska.

Frame, J., and P. Markowski, 2006: The interaction of simulated squall lines with idealized mountain ridges. *Mon. Wea. Rev.*, **134**, 1919–1941.

Keighton, S., J. Jackson, J. Guyer, and J. Peters, 2007: A preliminary analysis of severe quasi-linear mesoscale convective systems crossing the Appalachians. Preprints, *22nd Conf. on Weather Analysis and Forecasting*, Park City, UT, Amer. Meteor. Soc., 16 pp.

Letkewicz, C. E., and M. D. Parker, 2010: Forecasting the maintenance of mesoscale convective systems crossing the Appalachian Mountains. *Wea. Forecasting*, **25**, 1179–1195.

Letkewicz, C. E., and M. D. Parker, 2011: Impact of environmental variations on simulated squall lines interacting with terrain. *Mon. Wea. Rev.*, *in press*.

Morin, M. J., and M. D. Parker, 2011: A numerical investigation of supercells in landfalling tropical cyclones. *Geo. Res. Lett.*, **30**, L10801, doi:10.1029/2011GL047448, 2011.

NRCS, Soil Data Mart website, 2007. http://soildatamart.nrcs.usda.gov/Default.aspx

Parker, M.D. and D.A. Ahijevych, 2007: Convective episodes in the east-central United States. *Mon. Wea. Rev.*, **135**, 3707-3727.

Rotunno, R., J. B. Klemp, and M. L. Weisman, 1988: A theory for strong, long–lived squall lines. *J. Atmos. Sci.*, **45**, 463–485.

Schneider, D., and S. Sharp, 2007: Radar Signatures of Tropical Cyclone Tornadoes in Central North Carolina. *Wea. Forecasting*, **22**, 278–286.

Tang, Q. and L. Xie, 2008: Modeling inland flooding due to tropical cyclones. 28th Conference on Hurricanes and Tropical Meteorology, American Meteorological Society, Orlando, Florida, April 28-May 2, 2008.

Wang X and Melesse AM., 2006. Journal of the American Water Resources Association **42** (5): 1217-1236.

Weisman, M. L., and J. B. Klemp, 1982: The dependence of numerically simulated convective storms on vertical wind shear and buoyancy. *Mon. Wea. Rev.*, **110**, 504–520.